UNCLASSIFIED

AD 4 4 9 9 3 0

DEFENSE DOCUMENTATION CENTER
FOR
SCIENTIFIC AND TECHNICAL INFORMATION

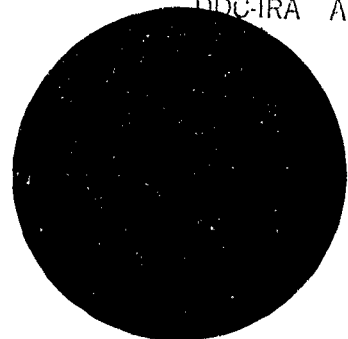CAMERON STATION ALEXANDRIA, VIRGINIA

UNCLASSIFIED

DISCLAIMER NOTICE

**THIS DOCUMENT IS BEST QUALITY
PRACTICABLE. THE COPY FURNISHED
TO DTIC CONTAINED A SIGNIFICANT
NUMBER OF PAGES WHICH DO NOT
REPRODUCE LEGIBLY.**

449930

DDC

OCT 26 1964

DDC-IRA   A

THE STRONG PLANE SHOCK PRODUCED
BY HYPERVELOCITY IMPACT
& LATE-STAGE EQUIVALENCE

by

P. C. Chou
H. S. Sidhu
L. J. Zajac

Drexel Institute of Technology
October, 1964

for presentation at the
Seventh Hypervelocity Impact Symposium
Tampa, Florida   November 17, 1964

PLANE SHOCK AND LATE-STAGE EQUIVALENCE

CONTENTS

ILLUSTRATIONS

PLANE SHOCK AND LATE-STAGE EQUIVALENCE

Page

PLANE SHOCK AND LATE-STAGE EQUIVALENCE

TABLES

PLANE SHOCK AND LATE-STAGE EQUIVALENCE

ABSTRACT

The attenuation of strong plane shocks produced by
hypervelocity impact is studied. Analytical equations are
developed which describe the path of the shock front. Since
the entropy change across the decaying shock is included in
the derivation, these equations are applicable to both weak
and strong shocks. The same problem is also solved graphically
by a stepwise characteristic method. The comparison of the
graphical and analytical results shows that the simplifying
assumptions made for the analytical solution are valid.

Calculations using our analytical equations show that
late-stage equivalence exists in one-dimensional like-material
impacts. Two impacts are equivalent if the quantity du_o^α is
the same for both cases. Here, α is between 1 and 2, and,
therefore, the basis of equivalence is between equal energy
and equal momentum.

It is also shown that the spall velocity can be consider-
ably higher than the impact velocity in hypervelocity like-
material impacts.

PLANE SHOCK AND LATE-STAGE EQUIVALENCE

SYMBOLS

c	Sound speed
d	Thickness of projectile
E	Specific internal energy
P	Pressure
t	Time
u	Particle velocity
U	Shock velocity
V	Specific volume
x	Distance
Z	$u + c$ sum of particle velocity and sound speed
ρ	Density
γ, A'	Parameters in the isentrope equation, Eq. 11.
a_1, a_2, a_3 b_1, b_2, b_3	Constants in Hugoniot equation (shock polars) Eqs. 17, 18.
ρ_o	Density at atmospheric conditions
P_o	Pressure on an isentrope where $\rho_o/\rho = 1$
U_p	Shock velocity in projectile (relative to ground)
U_t	Shock velocity in target (relative to ground)
T	Absolute temperature
R	Gas constant for ideal gas

PLANE SHOCK AND LATE-STAGE EQUIVALENCE

c_v Constant volume specific heat

c_p Constant pressure specific heat

γ Ratio of specific heats for ideal gas

$(\ )_0$ Undisturbed region in projectile

$(\ )_1$ Undisturbed region in target

$(\ )_2$ Region behind shocks (immediately after impact)

$(\ )_s$ Constant entropy

$(\ )_H$ Regions behind shocks or points on Hugoniot

Subscripted x or t refers to Figure 1

PLANE SHOCK AND LATE-STAGE EQUIVALENCE

I. INTRODUCTION

The most general problem in hypervelocity impact between
a finite cylindrical projectile and a semi-infinite target
involves three independent variables, i.e., axial distance,
radial distance, and time. Using essentially the finite-
difference methods, this problem has been successfully solved
in the hydrodynamic regime by Bjork,[1] Walsh, Johnson, Dienes,
Tillotson, and Yates,[2] and Riney.[3] Their methods involve the
introduction of an artificial viscosity with calculations per-
formed on high-speed computers. The results they obtain give a
most detailed numerical history of the properties and motions
of material particles.

In searching for an analytical solution, Rae and
Kirchner,[4] and Davids and Calvit,[5] have demonstrated that the
shock wave produced by impact and the flow field behind it pos-
sess approximate spherical symmetry and may be analyzed by
using only two independent variables, radius and time. Their
methods involve the assumption of similarity or quasi-similarity,
and the assumption of an ideal gas equation of state.

The simplest configuration in the study of hypervelocity
impact is the one-dimensional impact between two plates. It is
well known that the equation of state data are often

1

obtained from one-dimensional impact experiments, e.g., Walsh and Christian.[6] Recently, in the study of hypervelocity perforation of thin plates or bumper shields, the behavior of plane shocks and plane rarefaction waves have been shown to be of great importance. (See, for instance, Bull,[7] Maiden and Gehring,[8] and Sandorff.[9]) In addition to these practical applications, an understanding of plane waves is also helpful in the study of waves which are geometrically more complicated.

In the study of one-dimensional low-speed impact problems Herrman, et al,[10] have applied both the finite-difference method and the stepwise characteristic method and have given a detailed comparison of the merits of these two numerical methods. Due to the introduction of the artificial viscosity and the finite mesh size, they found that the finite-difference method does not produce a sharp shock front and the peak pressure is not accurate. Fowles[11] obtained an analytical expression for the decay of the plane shock front by using the characteristics method. Since he neglected the entropy change across the shock front, his results are valid only for weak shocks produced by low speed impacts.

In the present paper, the strong plane shock produced by hypervelocity impact is analyzed by two methods, both based

2

on the principles of characteristics. In the first method, certain simplifying assumptions are utilized, and two approximate analytical solutions are obtained. In the second method, a graphical stepwise characteristic approach is used. The results from these two methods demonstrate very close agreement. For low speed impacts, the present analytical solutions agree with Fowles' solution as expected. Under high speed impacts, however, the present solutions are considerably different from Fowles'.

The equations of state of metals used in this analysis are those obtained by Tillotson.[12] In order to facilitate the application of the characteristics method, a second order polynomial equation is fitted to the Hugoniot curve. Also, the isentropes are approximated by an equation similar to the one used by Murnaghan.[13]

According to numerical calculations of the present analytical solutions, late-stage equivalence exists for one-dimensional aluminum on aluminum impacts, if the product of the projectile plate thickness and its velocity raised to the α power is kept constant ($\alpha = 1.27$). For impacts between ideal gas ($\gamma = 1.4$), $\alpha = 1.5$ is shown to give one-dimensional late-stage equivalence, in agreement with the conclusion

3

PLANE SHOCK AND LATE-STAGE EQUIVALENCE

reached by Walsh, et al.

For low-speed impact of like materials, the free surface velocity (spall velocity) at the back of a thin target is equal to the original projectile velocity, provided the entropy change across the shock front is neglected. According to the equations of state data used in this paper, the spall velocity in aluminum is 7% higher (in copper, 14% higher) than the projectile velocity if the latter is around 20 km/sec.

The stepwise characteristics method is currently being extended to solve spherically symmetrical wave propagation problems on a digital computer. It is hoped that eventually this method may be applied to axially symmetrical problems. If successful, it would present a clear picture of the flow field in terms of shock waves, rarefaction waves, and path lines; the shock fronts and peak pressures would be accurately determined.

Most of the results in this paper are adopted from a report by the authors.[14] Recently, Allison[15] performed experiments on the attenuation of plane shock fronts in aluminum. His results, which compare favorably with the present solutions, will also be reported at this symposium.

PLANE SHOCK AND LATE-STAGE EQUIVALENCE

II.   STATEMENT OF THE IMPACT PROBLEM

A plate of thickness "d", which will be called the projectile, traveling at a velocity u_o in a direction normal to its plane surface, impacts a semi-infinite target plate of the same material at (x_o, t_o), as shown in Figure 1a. Two plane shock waves are generated, one in the target and the other in the projectile. The shock wave in the projectile reaches the free boundary at (x_1, t_1), and reflects from this point as a centered rarefaction wave. The head of this rarefaction wave reaches the collision boundary at (x_2, t_2) and overtakes the shock in the target at (x_3, t_3). From this point on, the rarefaction wave interacts with the shock, attenuating its velocity and peak pressure.

A solution to the problem involves a description of the state of the material behind the shock and an equation for the path of the shock front in the x-t plane. Certain simplifying assumptions to the problem are described in Section V, where the analytical solutions are given.

5

III. BASIC EQUATIONS

The method of characteristics in fluid mechanics and the governing equations for a normal shock are well known.[16, 17] In this section these basic equations are summarized for later use.

1. Normal Shock Equations

The equations expressing the conservation of mass, momentum, and energy across a shock are:

$$\rho_Y (U - u_Y) = \rho_x (U - u_x) \tag{1}$$

$$P_Y - P_x = \rho_x (U - u_x)(u_Y - u_x) \tag{2}$$

$$P_Y u_Y - P_x u_x = \rho_x (U - u_x)\left[E_Y - E_x + \tfrac{1}{2}(u_Y^2 - u_x^2) \right] \tag{3}$$

where U and u are the shock and particle velocities respectively, relative to ground (laboratory coordinates); P is pressure; ρ is density; and E is the specific internal energy. Subscripts x and y refer to the states ahead of and behind the shock front respectively. The equation of state of the material may be expressed as

$$P = P(E, \rho) . \tag{4}$$

If the condition ahead of the shock is known, then the quantities P_y, ρ_y, u_y, E_y, and U are related by the four equations, (1) to (4). Specification of any one of these variables will determine the remaining quantities. Alternately if the shock Hugoniot equation

$$P = P_H(\rho) \tag{5}$$

is known, then equations (1), (2), and (5) may be used to solve for any three of the four variables P_y, ρ_y, u_y, and U, in terms of the remaining variable. In applying the method of characteristics, construction of a c,u-state plane, or a P,u-state plane is necessary. The shock condition in the P,u-plane is represented by a "shock polar," which is a curve of P_y vs. u_y, obtained from equations (1), (2), and (5). If the relationship between c and P is known, a c,u-shock polar can also be constructed.

2. Characteristic Equations

The characteristic equations for unsteady, one-dimensional, isentropic flow are

$$\frac{dx}{dt} = u \pm c \tag{6}$$

$$d\rho \pm \frac{\rho}{c} du = 0 \tag{7}$$

7

where the upper and lower signs refer respectively to the C^+ characteristics (right traveling) and the C^- characteristics (left traveling). The sound speed c is defined by

$$c^2 = \left(\frac{\partial P}{\partial \rho}\right)_s \tag{8}$$

where the derivative is taken along an isentropic path. For isentropic flow,

$$dE = -P dV \qquad \left(V = \frac{1}{\rho}\right). \tag{9}$$

Substituting equation (9) into the general equation of state, equation (4), we obtain the isentropic P,ρ-relation (or isentrope).

$$P = P_s(\rho). \tag{10}$$

Equations (8) and (10) may be substituted into equation (7) to yield the state characteristic equation in the c,u-state plane. The state characteristics combined with the physical characteristics, equation (6), are the basic equations for the application of the method of characteristics.

It will be shown in the next section that the isentropes used in this report have the form

$$P = A'\left[\left(\frac{\rho}{\rho_o}\right)^{\gamma} - 1\right] + P_o. \tag{11}$$

8

This equation may be combined with (8) to yield

$$c^2 = \frac{A'\gamma}{\rho_0}\left(\frac{\rho}{\rho_0}\right)^{\gamma-1} = \frac{\gamma}{\rho}\left(P - P_0 + A'\right). \quad (12)$$

Equation (7) thus reduces to

$$\frac{2}{\gamma-1}\, dc \pm du = 0 \quad (13)$$

or

$$u \pm \frac{2c}{\gamma-1} = u_1 \pm \frac{2c_1}{\gamma-1} \quad (14)$$

which are the equations for the state characteristics. In the c,u-plane, these characteristics are straight lines with slopes $\pm 2/(\gamma-1)$. In the P,u-state plane the characteristics are

$$u \pm \frac{2\left(\frac{A'\gamma}{\rho_0}\right)^{\frac{1}{2}}}{\gamma-1}\left(\frac{P-P_0}{A'} + 1\right)^{\frac{\gamma-1}{2\gamma}} = \text{CONSTANT.} \quad (15)$$

IV. EQUATION OF STATE

For the present problem, the pressure in the solid material is of the order of 1/10 to 100 megabars. Under a pressure of this magnitude, the strength effect and the deviatoric components of stress can be neglected. One equation relating three state properties is sufficient to describe the state of the material. In other words, the material behaves like an ideal compressible fluid, and the equation of state is similar to that used in hydrodynamics.

PLANE SHOCK AND LATE-STAGE EQUIVALENCE

Under this hydrodynamic assumption, Tillotson obtained the following equation of state which is accurate for a large pressure range, (equation (6), Ref. 12).

$$P = \left[a + \frac{b}{\frac{E}{E_o \eta^2} + 1} \right] \frac{E}{V} + A\mu + B\mu^2 \qquad (16)$$

where P = pressure in megabars

E = specific internal energy in megabars-cm^3/gm

V = 1/ρ specific volume in cm^3/gm

η = ρ/ρ_o = V_o/V, where ρ_o is normal density, and

μ = η - 1

and a, b, A, B, E_o are constants dependent upon the metal. This equation is semi-empirical in nature and represents a best-fit extrapolation between Thomas-Fermi-Dirac data at high pressures (above 50 megabars) and shock wave experimental data at low pressures. This equation is accurate to approximately 5% of the Hugoniot pressure and 8% of the isentropic pressure.

Equation (16) is simple in form and is convenient for the numerical calculation of hypervelocity impact problems by the finite-difference methods. However, it is not suitable for an analytical solution to the present problem by the character-

istics method. A further simplification is incorporated by
fitting simple equations to the Hugoniot and isentropes of
equation (16).

Table I contains data for aluminum which is calculated
from the equation of state, equation (16), and the normal
shock conditions. (The detailed procedure is given in
Appendix A.) Two approaches have been used to fit the
Hugoniot data in Table I. In the first approach, the Hugoniot
is represented by a curve of U vs. Z, where $Z = u + c$. This
curve is fitted by the following equation,

$$U = a_1 + a_2 Z + a_3 Z^2 \qquad (17)$$

where the constants a_1, a_2, and a_3 are obtained by the method
of least squares. Figure 2a gives a comparison of equation
(17) with the data in Table I. The error is found to be less
than 1.0% in the range of 1 to 50 megabars. In the second
approach, an equation relating U and u,

$$U = b_1 + b_2 u + b_3 u^2 \qquad (18)$$

is obtained by the method of least squares. Figure 2b com-
pares equation (18) with the corresponding data in Table I.
The accuracy of this equation is within 0.4% for pressures with-
in the range of 1 to 50 megabars. Two different analytical

11

solutions for the shock path are developed in Section V.3, by using equations (17) and (18), respectively.

For the isentropes, an equation similar to Murnaghan's is assumed, i.e.,

$$P = A' \left[\left(\frac{\rho}{\rho_o} \right)^{\gamma} - 1 \right] + P_o . \qquad (11)$$

From any point on the P-V Hugoniot curve, an isentrope may be calculated from equation (16). Equation (11) is fitted to a number of these isentropes, and the constants A', γ, and P_o are determined; each of these constants assumes a different value for every isentrope. Table I gives values of these constants for aluminum. The accuracy of equation (11) as compared to equation (16) is very good as shown in Figure 3.

In the present report, the Hugoniot and isentrope equations are fitted to data presented in Ref. 6. Actually, Hugoniots of the form of equations (17) and (18) and isentropes of the form of equation (11) generally can be fitted to other equations of state data, theoretical or experimental.

V.   ANALYTICAL SOLUTIONS

1.   Assumptions

Besides the assumptions of a hydrodynamic equation of state and an adiabatic, non-viscous process, additional

12

assumptions are required to obtain an analytical solution for the decay of strong shocks. Fowles[11] assumed that the change of the entropy across the shock front is negligible, and thus his solution is limited to weak shocks. For strong shocks, the entropy change across the shock is appreciable and cannot be neglected.

Behind a strong shock the characteristic lines, to be exact, are not straight lines. However, the interactions between C^+ and C^- characteristics and between characteristics and contact lines are usually weak. In the present analytical approach, we assume that the characteristic lines in the rarefaction wave originating from point (x_1, t_1), Figure 1a, remain straight. Furthermore, either the particle velocity u, or the sum of particle velocity and sound speed $u + c$, is assumed constant along any one of these characteristic lines.

These assumptions are similar to those used in Ref. 18, which treats the decay of plane strong shocks in an ideal gas. The assumption of characteristic lines remaining straight has also been used by Al'tshuler, et al,[19] in an experimental technique to determine the sound velocity behind a strong shock. They have also performed numerical calculations to show that the error involved in their assumption of straight

13

characteristic lines is small, although the details are not given in their paper.

If the values of u are assumed constant along characteristic lines behind the shock front, the path of the shock can be determined from the exact shock equations. For points directly behind the shock front, the sound speed calculated from the exact shock equation is different from the sound speed on the same straight characteristic line near point (x_1, t_1). In the region immediately behind the shock front, therefore, this approach results in an inconsistency in sound speed, and consequently in pressure. The sound speed and pressure calculated from the shock equations are taken as the correct value behind the shock, and a linear variation in properties between the shock front and the rarefaction tail is assumed.

In the approach of $u + c$ = constant, the values of u and c singly are not assumed constant along the straight characteristic lines. The values of c and u behind the shock front are determined by the shock conditions, while a linear variation for these quantities is assumed between the shock and the tail of the rarefaction wave.

14

PLANE SHOCK AND LATE-STAGE EQUIVALENCE

2. Initial Conditions

According to eqs. (1) and (2), the shocks in the target and the projectile, immediately after impact, are governed by the conditions

$$\rho_1 U_t = \rho_2 (U_t - u_2) \qquad (19)$$

$$\left.\begin{array}{l} \\ \text{TARGET} \end{array}\right.$$

$$P_2 - P_1 = \rho_1 (U_t u_2) \qquad (20)$$

$$\rho_o (U_p - u_o) = \rho_2 (U_p - u_2) \qquad (21)$$

$$\left.\begin{array}{l} \\ \text{PROJECTILE} \end{array}\right.$$

$$P_2 - P_o = \rho_o (U_p - u_o)(u_2 - u_o) \qquad (22)$$

where the subscripts refer to regions in Figure 1b, and all velocities are relative to the ground (positive toward the right). Solving eqs. (19) to (22), we obtain the following relation

$$U_t = - (U_p - u_o) . \qquad (23)$$

This equation indicates that for impacts between like materials, the initial shock in the target and the shock in the projectile, have equal velocity with respect to the material ahead of each shock, but moving in opposite directions.

15

Equation (23) when substituted into eqs. (21) and (22), yields

$$\rho_1 U_t = \rho_2 (U_t - u_o + u_2) \qquad (24)$$

and

$$P_2 - P_1 = \rho_1 U_t (u_o - u_2) . \qquad (25)$$

Eliminating the pressure terms from eqs. (20) and (25) gives

$$u_2 = \frac{1}{2} u_o . \qquad (26)$$

Since U_t is equal to the magnitude of the velocity of the shock in the projectile relative to the undisturbed portion of the projectile, the time required for the shock to reach the free boundary is

$$t_1 - t_o = \frac{d}{U_t} . \qquad (27)$$

The absolute velocity of the shock in the projectile is $U_p = -U_t + u_o$; therefore, from Figure 1a,

$$X_1 - X_o = (t_1 - t_o)(-U_t + u_o) . \qquad (28)$$

By combining eqs. (19), (20), (26), (27), and (28), and using the geometry of the x,t-plane, we find that the head of the rarefaction wave reaches the collision boundary at time t_2, given by

$$t_2 - t_1 = (\rho_1 d) / (\rho_2 c_2) . \qquad (29)$$

16

PLANE SHOCK AND LATE-STAGE EQUIVALENCE

The interaction between the rarefaction wave and the shock front in the target starts at time t_3, which is given by

$$t_3 - t_2 = \frac{x_3 - x_2}{u_2 + c_2} = \frac{(t_3 - t_o)U_t - u_2(t_2 - t_o)}{u_2 + c_2}. \quad (30)$$

After simplification, equation (30) can be written as follows

$$t_3 - t_o = \frac{c_2(t_2 - t_o)}{u_2 + c_2 - U_t} \quad (31)$$

From (27) and (29), we obtain

$$t_2 - t_o = (t_2 - t_i) + (t_1 - t_o) = \frac{\rho_1 d}{\rho_2 c_2} + \frac{d}{U_t}. \quad (32)$$

Substituting for $(t_2 - t_o)$ from (32) in (31) yields

$$t_3 - t_o = \frac{c_2 d}{u_2 + c_2 - U_t}\left[\frac{\rho_1}{\rho_2 c_2} + \frac{1}{U_t}\right]. \quad (33)$$

The distance traveled by the shock before it is overtaken by the rarefaction wave is given by

$$x_3 - x_o = (t_3 - t_o)U_t = \frac{U_t c_2 d}{u_2 + c_2 - U_t}\left[\frac{\rho_1}{\rho_2 c_2} + \frac{1}{U_t}\right]. (34)$$

Up to the point (x_3, t_3), the shock front is a straight line. From this point on, the shock front becomes a curved line, and the shock strength attenuates.

For the present impact problem, the quantities x_o, t_o, d, u_o, ρ_1 and P_1, as well as the Hugoniot and isentropes of the material are all given. The particle velocity in region 2

17

u_2 is found from (26). The initial shock velocity U_t can be calculated from eq. (18), with u_2 substituted for u; c_2 and ρ_2 can then be determined from (12) and (24), or Table I, and then t_1, x_1, t_3, x_3 from (27), (28), (33), and (34), respectively.

3. Attenuation of the Shock

The shock attenuation is solved by two approaches. In the first approach, the characteristic lines in the x,t-plane are assumed as straight lines, and along each characteristic the sum of the particle and sound velocities, $u + c$, is assumed constant. In the second approach, these characteristic lines are again considered straight, but now only the particle velocity along each characteristic line is assumed constant.

a. "Constant u + c" Approach

A centered rarefaction wave starts at the point (x_1, t_1). Since the characteristic lines are assumed to be straight, the equation of a characteristic line originating from this point is

$$x - x_1 = (u + c)(t - t_1). \qquad (35)$$

After substituting $u + c = Z$, equation (35) becomes

$$x - x_1 = Z(t - t_1). \qquad (36)$$

PLANE SHOCK AND LATE-STAGE EQUIVALENCE

Differentiating both sides of this equation with respect to Z, we obtain

$$\frac{dx}{dZ} = (t - t_1) + Z\frac{dt}{dZ} . \tag{37}$$

Along the shock path, $dx/dt = U$, therefore we have

$$\frac{dx}{dZ} = \frac{dx}{dt}\frac{dt}{dZ} = U\frac{dt}{dZ} \tag{38}$$

where U is the shock propagation velocity.

From equations (37) and (38) we see that

$$U\frac{dt}{dZ} = (t - t_1) + Z\frac{dt}{dZ} . \tag{39}$$

Substituting the expression for U in terms of Z, equation (17), into equation (39), integrating and simplifying the resulting equation, we obtain

$$t = t_1 + (t_3 - t_1)\left[\frac{\alpha + Z}{\alpha + Z_2}\quad\frac{\beta + Z_2}{\beta + Z}\right]^{D/a_3} \tag{40}$$

where

$$\alpha = \frac{1}{2}\left[\sqrt{\left(\frac{a_2 - 1}{a_3}\right)^2 - \frac{4a_1}{a_3}} + \frac{(a_2 - 1)}{a_3}\right]$$

$$\beta = -\frac{1}{2}\left[\sqrt{\left(\frac{a_2 - 1}{a_3}\right)^2 - \frac{4a_1}{a_3}} - \frac{(a_2 - 1)}{a_3}\right]$$

and

$$D = \frac{1}{\beta - \alpha} .$$

19

PLANE SHOCK AND LATE-STAGE EQUIVALENCE

Equations (36) and (40) define the desired shock path in parametric form with Z as the parameter; t_1, t_3, x_1 and Z_2 are all known constants. In this approach, the only information used concerning the equation-of-state is the shock Hugoniot. The isentropes do not enter into this solution.

b. "Constant u" Approach

Following the manner of the previous section, the equation of a characteristic line starting from the point (x_1, t_1) can be written as

$$X - X_1 = (u + c)(t - t_1) \quad . \tag{41}$$

Also, for a characteristic line, according to equation (14)

$$u - \frac{2c}{\gamma - 1} = u_2 - \frac{2c_2}{\gamma - 1} \quad . \tag{42}$$

In this equation, γ is the constant in the isentrope eq. (11) for region 2 of Figure 4 (See Appendix A). Defining ℓ_1 as

$$\ell_1 = -\left(u_2 - \frac{2c_2}{\gamma - 1} \right) \tag{43}$$

we may rewrite equation (42) as

$$c = \frac{\gamma - 1}{2} \left(u + \ell_1 \right) .$$

Thus, from equation (41),

$$X - X_1 = \left(\frac{\gamma + 1}{2} u + \frac{\gamma - 1}{2} \ell_1 \right)(t - t_1). \tag{44}$$

20

Differentiating both sides of equation (44) with respect to u, we obtain

$$\frac{du}{du} = \frac{dx}{dt}\frac{dt}{du} = \frac{\gamma+1}{2}(t-t_1) + \left(\frac{\gamma+1}{2}u + \frac{\gamma-1}{2}l_1\right)\frac{dt}{du} . \quad (45)$$

Substituting eq. (18) into eq. (45), with $U = dx/dt$, we obtain

$$\left(b_1 + b_2 u + b_3 u^2\right)\frac{dt}{du} = \frac{\gamma+1}{2}(t-t_1) + \left(\frac{\gamma+1}{2}u + \frac{\gamma-1}{2}l\right)\frac{dt}{du} \quad (46)$$

or

$$\frac{dt}{t-t_1} = \frac{\gamma+1}{2}\frac{du}{b_3 u^2 + e_2 u + d_2} \quad (47)$$

where

$$e_2 = b_2 - \frac{\gamma+1}{2} \quad (48)$$

$$d_2 = b_1 - \frac{\gamma-1}{2}l_1 . \quad (49)$$

Integrating both sides of equation (47), we obtain

$$t = t_1 + \left(t_2 - t_1\right)\left[\frac{2b_3 u + e_2 - \sqrt{e_2^2 - 4b_3 d_2}}{2b_3 u + e_2 + \sqrt{e_2^2 - 4b_3 d_2}}\frac{2b_3 u_2 + e_2 + \sqrt{e_2^2 - 4b_3 d_2}}{2b_3 u_2 + e_2 - \sqrt{e_2^2 - 4b_3 d_2}}\right]^K$$

(50)

where $\qquad K = \frac{\gamma+1}{2\left(e_2^2 - 4b_3 d_2\right)^{1/2}} .$

Equations (50) and (44) represent the shock path in a parametric form, where u is the parameter. In this approach, in addition to the shock Hugoniot, one isentrope, or more precisely the γ in one isentrope, must be known for each impact problem; as can be seen from eqs. (42) and (43).

PLANE SHOCK AND LATE-STAGE EQUIVALENCE

4. Fowles' Solution

Fowles' weak shock solution is given below for the purpose of comparison. His equations for the path of the shock front are

$$t(\sigma) = t_1 + (t_3 - t_1)\left[\frac{\sigma_0}{\sigma_0 - 2(\gamma' + 1)}\right]^2\left[\frac{\sigma - 2(\gamma' + 1)}{\sigma}\right]^2_{(t > t_3)} \qquad (51)$$

and

$$X(\sigma) = X_1 + c_1(\sigma + 1)(t_3 - t_1)\left[\frac{\sigma_0}{\sigma_0 - 2(\gamma' + 1)}\right]^2\left[\frac{\sigma - 2(\gamma' + 1)}{\sigma}\right]^2_{(t > t_3)} \qquad (52)$$

where γ' is a constant depending on the material (4.266 for aluminum), and σ is the parameter defined by

$$\sigma = \frac{u + c}{c_1} - 1$$

and

$$\sigma_0 = \frac{X_3 - X_1}{c_1(t_3 - t_1)} - 1 .$$

He used eq. (11) with one set of constants as both the isentrope and the Hugoniot for calculating the initial conditions.

VI.   GRAPHICAL SOLUTIONS

The graphical solution of the present problem is obtained
by using the "field method" procedure of the theory of
characteristics as described in Ref. 17.   Although this
method is time consuming, it yields a very accurate solution
which may be used as a basis of comparison for the approximate
analytical solutions.

This method involves the use of three planes, the physical
plane ($c_1 t$,x-diagram of Figure 4), the P,u-state plane
(Figure 5a) and the c,u-state plane (Figure 5b).   A region
of continuously varying fluid properties in the physical plane
is replaced by a number of finite regions each having uniform
fluid properties.   These regions are separated by three types
of lines, namely, the shock front, the characteristics, and
the contact lines.

In the present problem two shock fronts appear in the
physical plane, but only one shock polar is required
in each state plane.   These shock polars are plotted in the
c,u-state plane by using the data of c_H vs. u in Table I,
while in the P,u-plane by P_H vs. u.

23

PLANE SHOCK AND LATE-STAGE EQUIVALENCE

Equation (14), in the following form, is used to plot the c,u-characteristics

$$\left[u \pm \frac{2c}{\gamma - 1} = u_H \pm \frac{2c_H}{\gamma - 1} \right]_{I,II} \qquad (14)$$

where c_H and u_H are the properties in the region immediately behind the shock, u and c are the properties in isentropically connected regions, and γ is determined from Table I. These characteristics are straight lines with slopes

$$\left[\frac{dc}{du} = \mp \frac{\gamma - 1}{2} \right]_{I,II} \quad .$$

Equations 11, 12, and 14 are combined to yield the P,u-characteristics

$$\left[u \pm \frac{2}{\gamma - 1} \left(\frac{A'\gamma}{\rho_o} \right)^{\frac{1}{2}} \left(\frac{P - P_o}{A'} + 1 \right)^{\frac{\gamma - 1}{2\gamma}} = u_H \pm \frac{2c_H}{\gamma - 1} \right]_{I,II} \qquad (15.a)$$

where $u_H \pm 2c_H/(\gamma - 1)$ is a constant for regions of equal entropy and depends on the properties of the region behind the shock. The constants A', γ, P_o, and c_H may also be obtained from Table I.

The P,u-state plane is used in the graphical solution because it facilitates the determination of the physical properties in regions bounding contact lines. Two regions bounding a contact line have identical pressures and particle

24

velocities and therefore plot as a single point in this plane. The c,u-state plane yields the required sound velocity which is needed in constructing the physical $c_1 t$,x-diagram.

The initial position of the right traveling shock in the physical plane is constructed with the slope c_1/U_t, and the left traveling shock with slope c_1/U_p. The slopes of the physical characteristics are given by

$$\left[\frac{d(c_1 t)}{dx} = \frac{c_1}{u \pm c} \right]_{I,II}$$

where the upper sign refers to the I-characteristic (C^+ or right-traveling waves) and the lower sign refers to the II-characteristics (C^- or left-traveling waves). Both the sound velocity c and particle velocity u represent the average between their respective values on both sides of the characteristic line.

The simple rarefaction wave centered at $(c_1 t_1, x_1)$ is arbitrarily divided into regions by assuming approximately equal increments of particle velocity between adjacent regions, as shown in Figure 4. These waves are propagated with constant strength until the head of the rarefaction wave overtakes the shock front. As the shock continues with decreased strength and velocity, contact lines and reflected waves are formed.

25

PLANE SHOCK AND LATE-STAGE EQUIVALENCE

A contact line, which separates regions of unequal entropy, forms because the fluid particles passing through shocks of unequal strength attain different levels of entropy. A reflected wave is required in order to satisfy the boundary conditions of equal pressure and equal particle velocity across a contact line. All the regions bounded by the shock path and a pair of neighboring contact lines are at the same entropy level; therefore the coefficients A', γ, and P_o which are used in the characteristic equations are constant within each of these regions. When crossing a contact line, new values for A', γ, and P_o must be selected from Table I.

The properties of regions 1 and 2 are determined by the initial conditions of the problem. From the assumed particle velocities in regions 3 to 9, the pressures and sound velocities can be determined from the characteristic lines passing through point 2 in the c,u-plane and the P,u-plane. Regions on both sides of a contact line have equal pressures and particle velocities, (i.e., the pressure and particle velocity in regions 10 and 20 are equal). Therefore the points 10 and 20 in the P,u-state plane coincide. In the c,u-plane, Figure 5, point 10 lies directly above point 20. Similarly, regions 21 and 30 plot as a single point in the

26

P,u-state plane and lie at the intersection of a I-character-
istic through point 11 and II-characteristic through point 20.

For a complete and detailed discussion of the graphical
method of solution, the reader is referred to Refs. 16, 17,
and 18.

As an example of the graphical method applied to the
present problem, an aluminum on aluminum impact was chosen,
with d = 3.175 mm and u_o = 28.2 km/sec. Figure 4 shows the
results in the physical plane and Table II gives the calcu-
lated physical properties in selected regions.

VII. COMPARISON OF RESULTS

In this section the results of the two analytical
approaches will be compared. The analytical results will then
be compared with the graphical solution and Fowles' solution.
The paths of the shock as obtained by the two analytical
approaches, "constant u" and "constant u + c", are shown in
Figure 6. For small values of time the two assumptions yield
identical paths; for large values of time, the paths diverge
progressively. The relative accuracy of these two approaches
can be evaluated from the c,u-state plane in the graphical
solution as shown schematically in Figure 7a. Numbered

27

points in this figure refer to corresponding regions in
Figure 4. The exact properties in regions 2, 4, and 20 as
determined by the graphical method are represented by the
points 2, 4, and 20, respectively, in Figure 7a. According
to the "constant u" approach, the particle velocity in region
20, u_{20}, is equal to that in region 4, u_4. Therefore, the
properties in region 20 are represented in Figure 7 by point
20': the intersection of the vertical line through point 4
and the shock polar. According to the "constant u + c"
approach

$$u_{20} + c_{20} = u_4 + c_4 . \tag{53}$$

Thus region 20 is represented in Figure 7a by point 20": the
intersection of the straight line plotted from equation (53)
and the shock polar. (Equation (53) is a straight line
inclined at 45° from the axes if c and u are plotted in the
same scale.) An inspection of Figure 7a shows that point 20"
is much closer to point 20 than is point 20'. A similar dis-
cussion can also be made for points 5, 70, 70', and 70". The
"constant u + c" approach can be expected, therefore, to be
more accurate than the "constant u" approach.

Another way of evaluating the relative accuracy of these
two approaches is to compare the change in u and u + c

between two regions, one immediately behind the shock and one in the simple wave region, such as regions 20 and 4 or regions 70 and 5, in Figure 4. Table 3a shows the results of such a comparison. The percentage change in u between regions 6 and 120 is -1.67, while the percentage change in u + c is only 0.300. Thus "constant u + c" is seen to be a better approximation than the "constant u."

The discussion in the preceding paragraphs is true for aluminum only. No conclusion has been reached for metals in general. It is interesting to note that calculations made for an ideal gas with a ratio of specific heat of 1.4 indicate an opposite trend. That is, the "constant u" approach is more accurate than the "constant u + c" approach, as demonstrated by Figure 7b and Table 3b. Figure 7b is constructed in the same manner as Figure 7a and with the points similarly numbered. The major difference between the two is that for the ideal gas, Figure 7b, the shock polar is below the II-characteristic line in the region of points 2, 4, and 5. Primarily due to this change in the relative position of the shock polar and characteristics, the trend in the accuracy of the two approaches is reversed. Table 3b is calculated in the same manner as Table 3a. The equivalent impact velocity used

29

for the ideal gas is 1.22 km/sec, and the ratio of specific
heat is taken as 1.4.

For weak shocks, the paths of the decaying shock obtained
from all three methods (analytical, graphical and Fowles')
fall on one curve. For strong shocks, the present analytical
solution is in close agreement with the graphical solution,
whereas Fowles' solution deviates considerably from the other
two, as shown in Figure 8a.

For high impact velocities (above 22 km/sec) the shock
from the present analytical solution lies above the one cal-
culated from Fowles' solution, as shown in Figure 8a. For
low impact velocities, however, the relative position of the
shock front is just the opposite, i.e., the present solution
is below Fowles', as shown in Figure 8b.

Figure 9 gives the comparison of peak pressure distri-
butions for the aluminum-on-aluminum impact by the graphical
method and by the "constant u + c" approach.

VIII. LATE-STAGE EQUIVALENCE

The principle of late-stage equivalence, as proposed by
Walsh, et al,[2] stipulates that projectiles of differing mass
and velocity can give rise to target flows which are very

30

nearly identical at late times, provided the product of the mass and the velocity raised to the 3α power $(M_o u_o^{3\alpha})$ is the same for all projectiles. For one-dimensional impacts, they showed that the late-stage equivalence on the basis of du_o^{α} leads to the result that the flow is of the self-similar type. The analytical similarity solution and a solution by finite-difference calculations (Sputter Code) of an impact in ideal gas, with $\gamma = 1.4$, are in excellent agreement at late times.

In this section, this similarity solution for an ideal gas is compared with the approximate, analytical equation derived by the "constant u" approach. In addition, late-stage equivalence for like-material impacts in aluminum and copper is studied by the "constant u + c" approach.

The "constant u" approach is used for an ideal gas because it is more accurate than the "constant u + c" approach as discussed in the previous section. The detailed equations used are summarized in Appendix B. The particular similarity solution being compared has the following constants:

$$\gamma = 1.4$$
$$\alpha = 1.5$$
$$du_o^{1.5} = 1.2 \times 10^9 \ (cm^2/sec)^{1.5} \qquad (= L_o v_o^{\alpha} \text{ of Ref. 2})$$

31

PLANE SHOCK AND LATE-STAGE EQUIVALENCE

The similarity solution is compared with two impact cases having the same du_o^α, but different u_o. The resulting shock position in the t-(x + d) plane is presented in Figure 10 and the corresponding peak pressure vs. (x + d) curves are shown in Figure 11. The distance x + d is measured from the free-surface of the projectile at the instant of impact, while x is measured from the free-surface of the target, both in Eulerian coordinates. Thus x + d is equivalent to the Lagrangian distance hV_o in Ref. 2.

The positions of the shock front, for the two impact cases and the similarity solution, agree very well. The peak pressure comparison is fairly good. The approximate analytical solution, when carried to very late times, involves an increasing amount of error, thus it is not suitable for very late-stage comparison.

Figures 12 to 13 show the late-stage equivalence, for one-dimensional aluminum-on-aluminum impacts, according to the "constant u + c" approach. These impacts show surprisingly good agreement with a single value of α, 1.27. The late-stage equivalence is not too sensitive to the exact value of α. Satisfactory comparison can be obtained for impacts with values of α from 1.25 to 1.3.

PLANE SHOCK AND LATE-STAGE EQUIVALENCE

Figure 14 shows the late-stage comparison for like-material impact in copper. The value for α used is 1.7, while the range of satisfactory values is from 1.6 to 1.8.

As mentioned before, the present analytical solution is not too accurate at a very late-stage. But due to the simplicity of the solution, it can be used conveniently for comparison of many impact situations. Up to a point where the peak pressure is one-quarter of the value of the initial peak pressure, the analytical solution is fairly accurate. By using the solution up to this point, the principle of late-stage equivalence is shown to exist for one-dimensional impacts. For the materials considered, the equivalence is neither on the basis of projectile momentum, nor on the basis of energy, but somewhere in between.

Walsh, et al,[2] have shown that for axisymmetrical impacts, one value of the late-stage equivalence exponent, $3\alpha = 1.74$, holds for all materials including metals and ideal gases with different values of γ. From one-dimensional similarity considerations, they have concluded, however, that for ideal gas the exponent α is not constant but varies from 1.0 to 1.79 as γ is varied from 1.0 to infinity. For one-dimensional impacts, we have also demonstrated that the late-stage equivalence

33

exponent α assumes different values for different materials; 1.27 for aluminum, 1.7 for copper, 1.5 for ideal gas with $\gamma = 1.4$. The fact that one α holds for all materials in axi-symmetric impacts while a different value of α must be used for each material in one-dimensional cases can be explained by the following reasoning. The attenuation of the shock front produced in a three-dimensional impact is due to two factors: the space attenuations and the attenuations by the rarefaction wave originated from the free surface. In a one-dimensional impact, only the latter (rarefaction wave effect) exists and there is no space attenuation. It is plausible to assume that the space attenuation is independent of the material equation of state while it is known that the rare-faction wave does depend on the material property. The results of late-stage equivalence indicates that in the three-dimensional case, the space attenuation predominates and therefore one value of α is applicable for all materials. In one-dimensional impact where only the rarefaction wave effect exists, each material possesses a different value of α.

It must be realized that the whole concept of late-stage equivalence is not based on a rigorous theoretical formulation. Even in the case of one-dimensional impact for an ideal gas,

there is no reason why the shock wave due to impact should behave like the similarity solution at late stage. The similarity solution satisfies all the governing equations in the flow field, it satisfies the boundary condition across the shock, as well as the boundary condition of zero pressure at the free-surface. But it does not satisfy the initial conditions due to impact. The condition of constant total energy, constant total momentum, or constant du_o^α , does not constitute a precise initial condition required by the governing differential equations. It is only fortunate that impact calculations do agree with the similarity solution at late stage and demonstrate a late-stage equivalence.

IX. SPALL VELOCITY IN THIN TARGETS

One of the methods used to experimentally determine the shock Hugoniot for metals is to impact a thin target plate with a thick projectile plate. When the shock front in the target reaches the free-surface, it reflects as a centered rarefaction wave. The particles at the free-surface are accelerated by this rarefaction wave to a velocity u_{sp}, called the spall velocity or free-surface velocity. Let u_r be the velocity due to the rarefaction wave and u_2 be the particle

velocity behind the shock front. Then,

$$u_{sp} = u_2 + u_r$$

If the entropy change across the shock front is neglected, the Hugoniot and isentrope curves coincide. As a result, for like-material impacts

$$u_r = u_2 \quad \text{and} \quad u_{sp} = 2u_2 = u_o$$

For low speed impacts, the neglect of entropy change does not introduce any appreciable amount of error. Walsh[6] and Christian have shown, that for peak pressures less than 400 kilobars in aluminum (u_o < 4 km/sec), the error involved in assuming $u_r/u_2 = 1$ is less than 2%.

For higher impact velocities, the entropy change cannot be neglected and the actual spall velocity can be much higher than the impact velocity. For instance, at an impact velocity of 20 km/sec in aluminum, according to the equation of state data given in Table I, the ratio u_r/u_2 is 1.14, 14% higher than unity.

The method of determining the spall velocity can be best demonstrated by using curves in the P,u-state plane, as shown in Figure 15. Figure 15a is for aluminum-on-aluminum impacts, while Figure 15b is for copper-on-copper. Although the

36

relative positions of the curves in these two figures are slightly different, the discussion to follow can be applied to both of them. Point 1, with $P_1 = u_1 = 0$, represents the properties of the undisturbed target, while point 3 represents the properties of the projectile before impact. After impact, the properties of the material between the two shocks are represented by point 2, which is at the intersection of the right-traveling and left-traveling shock polars. After reaching the free-surface of the target, the shock is reflected as a centered rarefaction wave, which is represented by the I-characteristic in Figure 15. The spall velocity is then given by the intersection of this characteristic and the u-axis, shown as point 4. It can be seen that $u_{sp} > u_o$ for both aluminum and copper. If entropy is neglected, the shock polar and characteristics coincide. Thus the properties in the target vary continuously from point 2 to point 3, resulting in a spall velocity equal to the impact velocity.

For a thin projectile, when the shock in the projectile reaches the free-surface, the "back-splash" can also be determined from this figure. From the condition behind the shock, point 2, the rarefaction follows the II-characteristic to zero pressure at point 5, which gives the back-splash

37

velocity u_{bs}. Since, for like-material impacts, the shocks and characteristics in this figure are symmetrical with respect to the vertical line through point 2, it is evident that

$$u_{bs} = u_{sp} - u_o$$

If the entropy change is neglected, the rarefaction in the projectile would follow the shock polar and point 5 would coincide with point 1. Under this condition, the free surface of the projectile attains zero velocity.

The results calculated for a few like-material and different-material impacts are shown in Figure 16, where the spall velocity u_{sp} is plotted as a function of the impact velocity u_o. For like-material impacts, u_{sp} is larger than u_o for copper and beryllium, as well as for aluminum. For different-material impacts, the spall velocity may be higher or lower than the impact velocity, depending on the density ratio between the target and the projectile. More specifically, for the materials studied in these impact cases, we have

$$u_{sp} > u_o \qquad \text{if} \qquad \rho_{proj.}/\rho_{target} \geq 1$$

The detailed equations used for these calculations are given in Appendix C.

PLANE SHOCK AND LATE-STAGE EQUIVALENCE

X. CONCLUSIONS

1. Closed form equations have been obtained which give the path of the shock front due to one-dimensional hypervelocity impact. In deriving these equations, entropy changes have been included, thus they are applicable to both weak and strong shocks. The accuracy of these equations are good up to a point on the shock front where the peak pressure is approximately one-quarter of the original peak pressure. For low-speed impacts where the shocks are weak, these equations give the same results as those of Fowles' which neglect the entropy change. For high-speed impacts where the shocks are strong, the shock front predicted by the present analytical equations are considerably different from those predicted by Fowles' solution.

2. According to the analytical formulas in this report, late-stage equivalence exists for one-dimensional like-material impacts. The exponent α is 1.27 for aluminum, 1.70 for copper, and 1.5 for ideal gas ($\gamma = 1.4$). These numbers lie between 1.0 and 2.0 which are the constant momentum scaling and constant energy scaling factors, respectively.

PLANE SHOCK AND LATE-STAGE EQUIVALENCE

3. For impacts between a thick projectile and a thin target
of like materials, the spall velocity is considerably higher
than the projectile velocity for high-speed impacts. The
widely used assumption that the spall velocity is equal to the
projectile velocity is thus inaccurate for impact velocities
above 10 km/sec.

4. Equation-of-state data for metals may be conveniently
described by simplified Hugoniot and isentrope equations, (17)
or (18) and (11). With these equations, rarefaction waves and
shock waves including entropy changes can be studied by the
method of characteristics.

5. The stepwise calculation by the method of characteristics,
as compared with the finite-difference method with artificial
viscosity, can sometimes shed more light on the mechanism of
the flow field. It can give more precise locations of the
shock fronts and give more accurate values of peak pressures.
In the solutions by finite-difference methods, pressures are
sometimes poorly defined, oscillations occur in the pressure
profile (as much as 15%), and the shock fronts are smeared out
at late times, as pointed out in Ref. 2. In Ref. 3, by the

finite-difference method, the spall velocity is shown to equal
the impact velocity for aluminum at 20 km/sec, in contradiction
with the result in this paper.

However, whether the stepwise characteristic method can
be applied to the two-dimensional impact problems remains to
be seen.

PLANE SHOCK AND LATE-STAGE EQUIVALENCE

REFERENCES

1. Bjork, R. L., "Review of Physical Processes in Hypervelocity Impact and Penetration," Proc. of the Sixth Symposium on Hypervelocity Impact, August 1963, Vol. II, Part I.

2. Walsh, J. M., Johnson, W. E., Dienes, J. K., Tillotson, J. H., and Yates, D. R., "Summary Report on the Theory of Hypervelocity Impact," GA-5119, General Atomic, General Dynamics, San Diego, California, March 1964.

3. Riney, T. D., "Theoretical Hypervelocity Impact Calculations Using the Picwick Code," R64SD13, Space Sciences Laboratory, General Electric, February 1964.

4. Rae, W. J., and Kirchner, H. P., "A Blast-Wave Theory of Crater Formation in Semi-infinite Targets," Proc. of the Sixth Symposium on Hypervelocity Impact, August 1963, Vol. III, pp. 163-228.

5. Davids, N., Calvit, H. H., and Johnson, O. T., "Spherical Shock Waves and Cavity Formation in Metals," Proc. of the Sixth Symposium on Hypervelocity Impact, August 1963, Vol. III, pp. 229-272.

6. Walsh, J. M. and Christian, R. H., "Equation of State of Metals from Shock Wave Measurements," Physical Review, March 1955, Vol. 97, No. 6.

7. Bull, G. V., "On the Impact of Pellets with Thin Plates. Theoretical Considerations Part I," A. D. Little, Inc., Report No. 63270-03-01, 1962.

8. Maiden, C. J., Gehring, J. W., and McMillan, A. R., "Investigation of Fundamental Mechanism of Damage to Thin Targets by Hypervelocity Projectiles," Final Report TR 63-225, Defense Research Laboratories, General Motors Corp., Santa Barbara, California, September 1963.

9. Sandorff, P. E., "A Meteoroid Bumper Design Criterion," Proc. of the Sixth Symposium on Hypervelocity Impact, August 1963, Vol. III, pp. 41-68

10. Herrmann, W., Witner, E. A., Percy, J. H., and Jones, A. H., "Stress Wave Propagation and Spallation in Uniaxial Strain," ASD-TDR-62-399, AF Systems Command Wright Patterson Air Force Base, September 1962.

11. Fowles, G. R., "Attenuation of the Shock Wave Produced in a Solid by a Flying Plate," Jour. Applied Physics, April 1960, Vol. 31, No. 4, pp. 655-661.

12. Tillotson, J. H., "Metallic Equations of State for Hyper-velocity Impact," GA-3216, General Atomic, July 18, 1962.

13. Murnaghan, F. D., Finite Deformation of an Elastic Solid, John Wiley and Sons, Inc., New York, 1951.

14. Chou, P. C., Sidhu, H. S., and Zajac, L. J., "Attenuation of the Strong Plane Shock Produced in a Solid by Hyper-velocity Impact," D.I.T. Report No. 125-5, Drexel Inst. of Technology, Philadelphia, Pennsylvania, February 1964.

15. Allison, F. E., "Attenuation of Plane Shock Fronts in Aluminum," To be published as a Ballistic Research Laboratories Report. See Also, Allison, F. E., "Mechanics of Hypervelocity Impact," A paper to be presented at the Seventh Hypervelocity Impact Symposium, November 1964.

16. Courant, R., and Friedrichs, K. O., Supersonic Flow and Shock Waves, Interscience Publishers, Inc., New York, 1948.

17. Shapiro, A. H., The Dynamics and Thermodynamics of Compressible Fluid Flow, Vol. II., The Ronald Press Company, New York, 1954.

18. Chou, P. C., Karpp, R. R., and Zajac, L. J., "Decay of Strong Plane Shocks in an Ideal Gas," D.I.T. Report No. 160-3, Drexel Institute of Technology, Philadelphia, Pennsylvania, January 1964. Also appears as NASA CR-107, Sept., 1964.

19. Al'tshuler, L. V., Kormer, S. B., Brazhnik, M. I., Vladimirov, L. A., Speranskaya, M. P., and Funtikov, A. I., "The Isentropic Compressibility of Aluminum, Copper, Lead, and Iron at High Pressures," Soviet Physics JETP, October 1960, Vol. II, No. 4.

20. Walsh, J. M., Rice, M. H., McQueen, R. G., and Yarger,F.L., "Shock-Wave Compressions of Twenty-Seven Metals. Equations of State of Metals." Physical Review, October 1957, Vol. 108, No. 2. See Also, Rice M. H., McQueen, R. G., and Walsh, J. M., "Compression of Solids by Strong Shock Waves," Solid State Physics, 1958, Vol. 6.

21. Sedov. L. I., Similarity and Dimensional Methods in Mechanics, Academic Press, New York and London, 1959.

22. Taylor, G. I., "The Formation of a Blast Wave by a Very Intense Explosion, I. Theoretical Discussion," Proc. Roy. Soc. A, March 1950, Vol. 201, P. 159.

(a)

PROJECTILE TARGET

$U_p(< u_o)$

u_o u_2 u_2 U_t

u_2 $u_i = 0$

$\rho_o = \rho_i$ ρ_2 ρ_2 ρ_i

$P_o = P_i$ P_2 P_2 P_i

BACK SURFACE SHOCK INTERFACE SHOCK
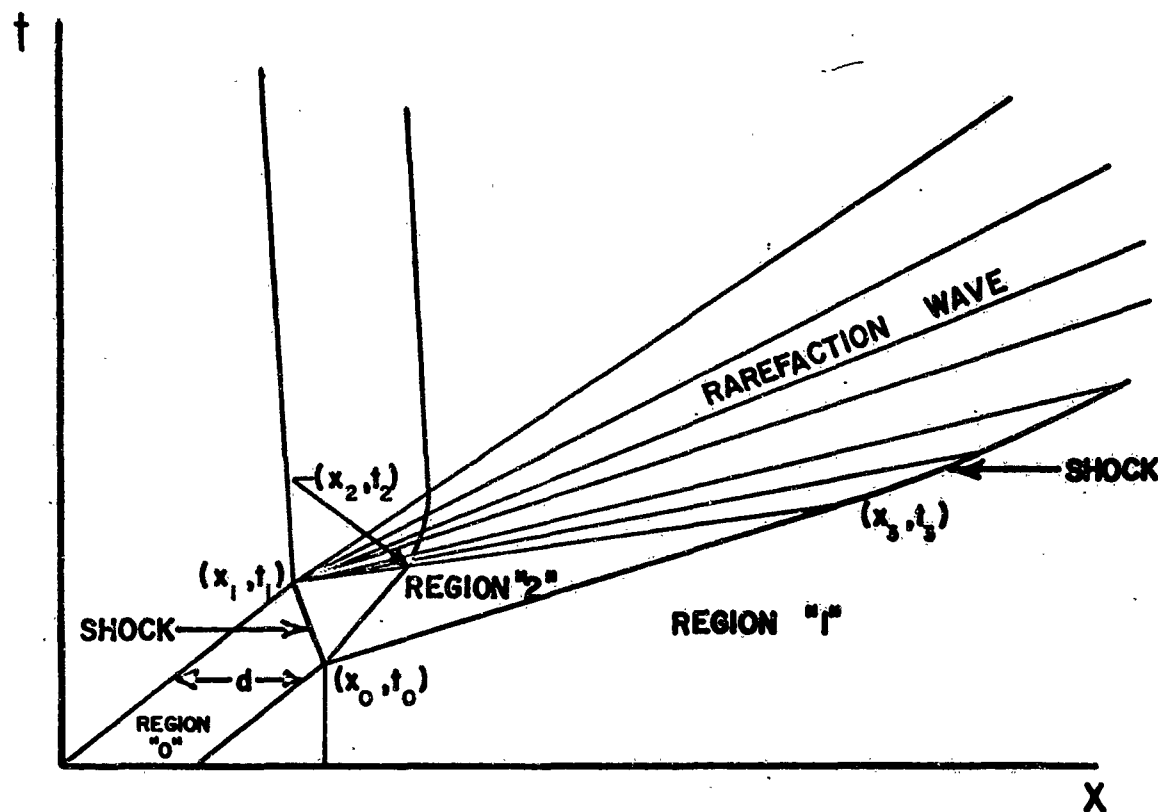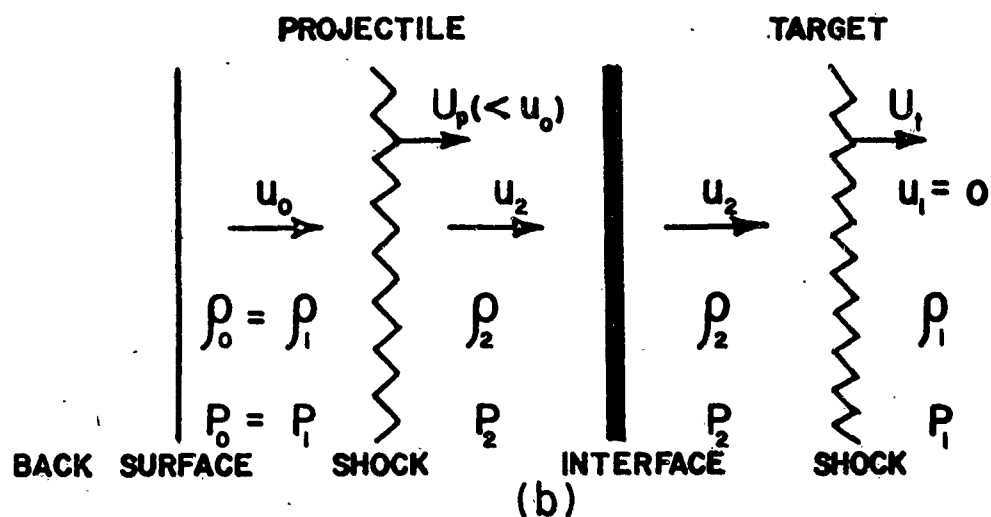
(b)

Figure 1. Plane Shocks Due to Impact
a. Physical Plane (Schematic)
b. Initial Configuration
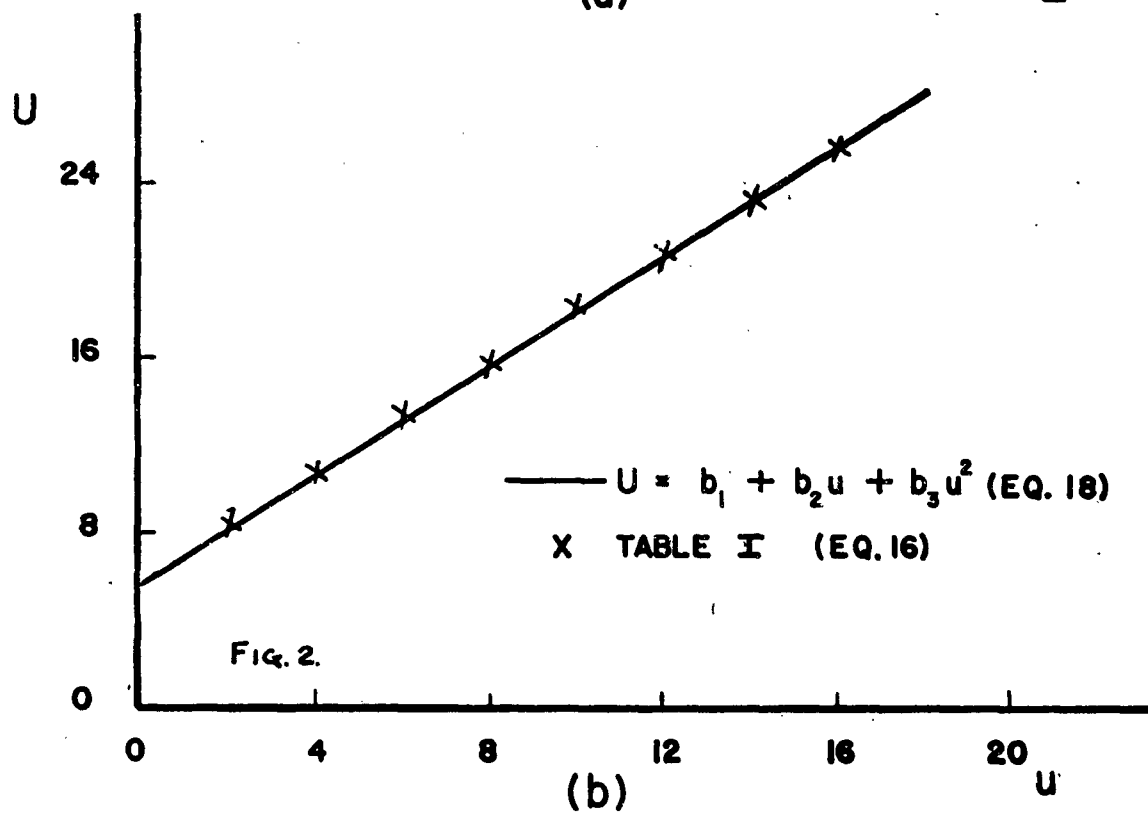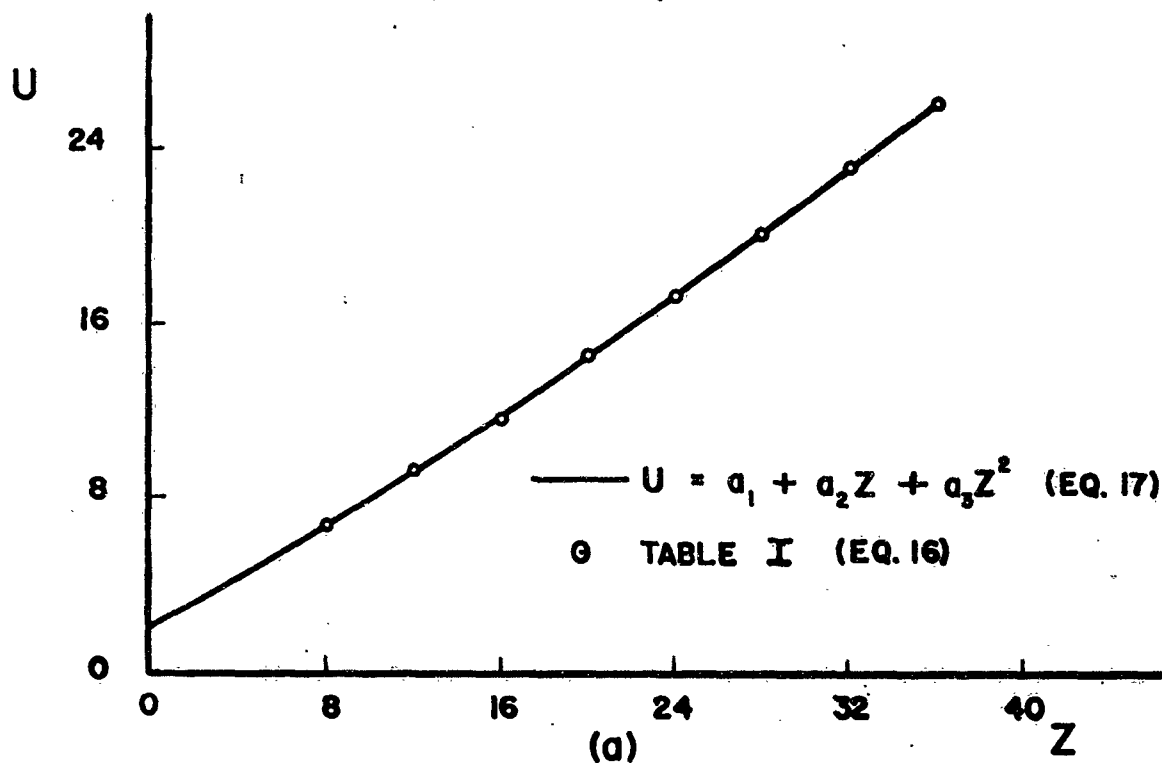
Figure 2.   Comparison of "Shock Polars" eqs. 17 and 18, with
             Tillotson's Data, Eq. 16.
             a. $U = a_1 + a_2 Z + a_3 Z^2$
             b. $U = b_1 + b_2 u + b_3 u^2$

PLANE SHOCK AND LATE-STAGE EQUIVALENCE
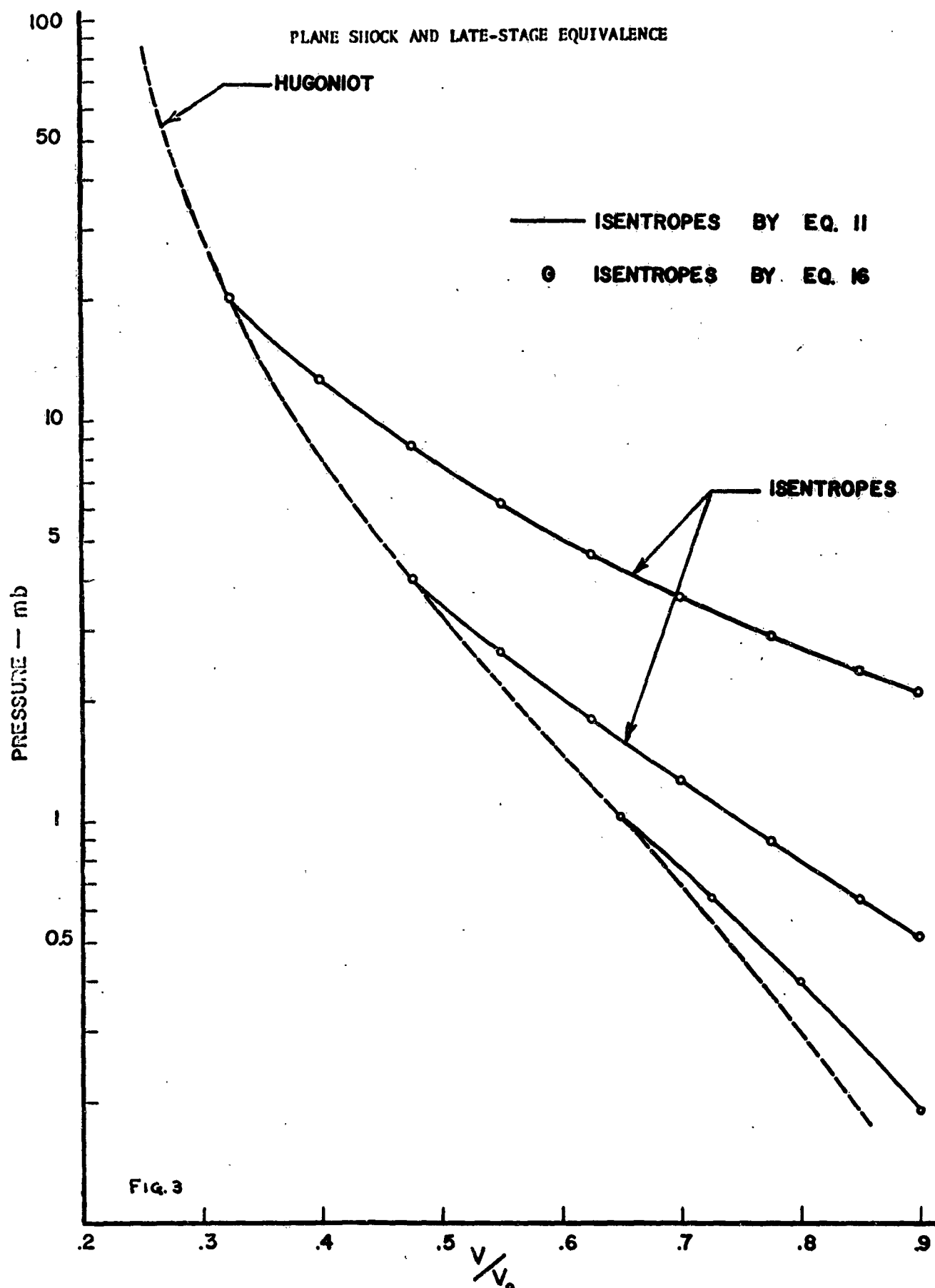
Figure 3.   Comparison of Isentropes, eq. 11, with Tillotson's Data, Eq. 16.   47

FIG. 4.
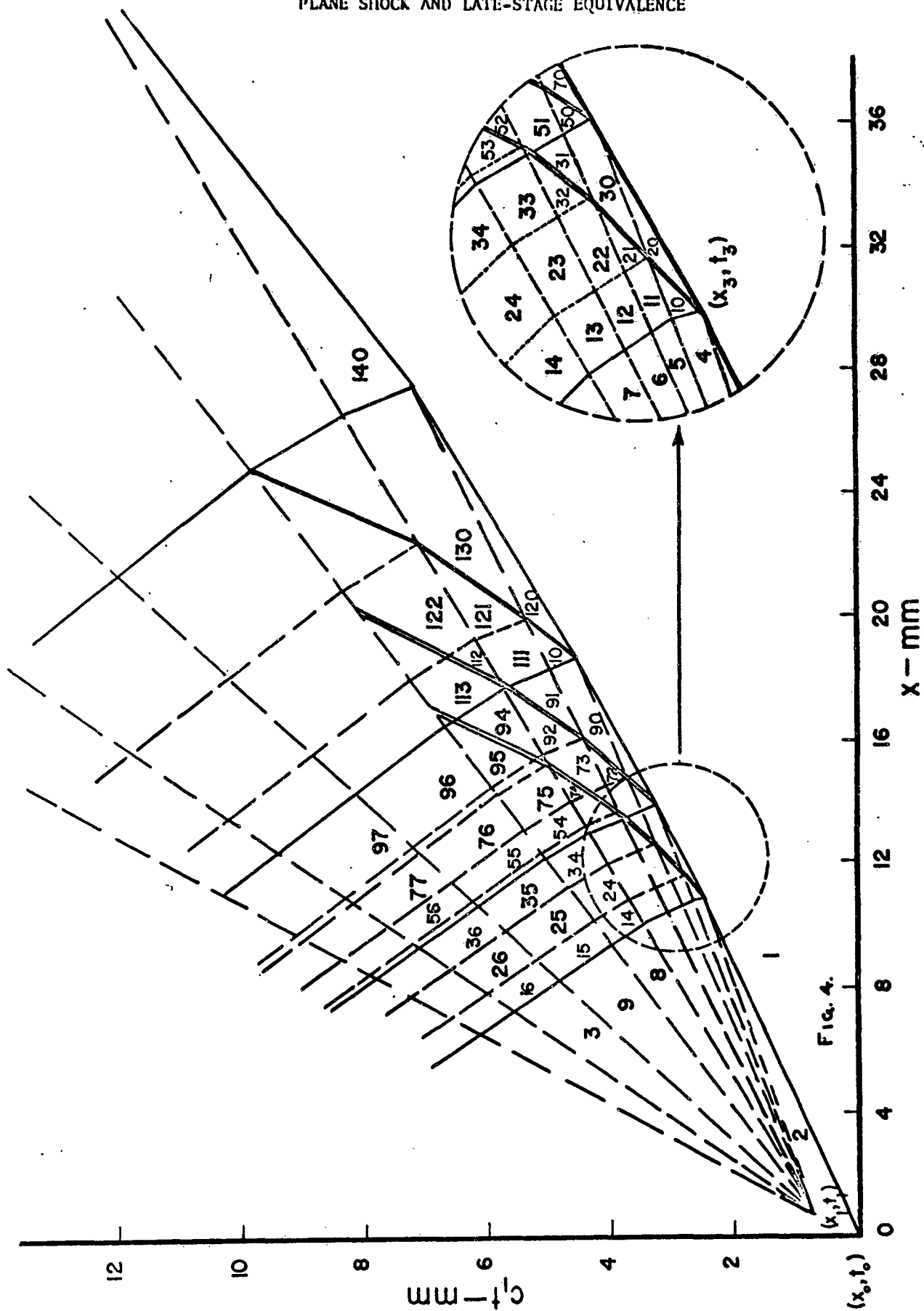
Figure 4.   Regions in the Physical Plane Used in the Graphical Solution.
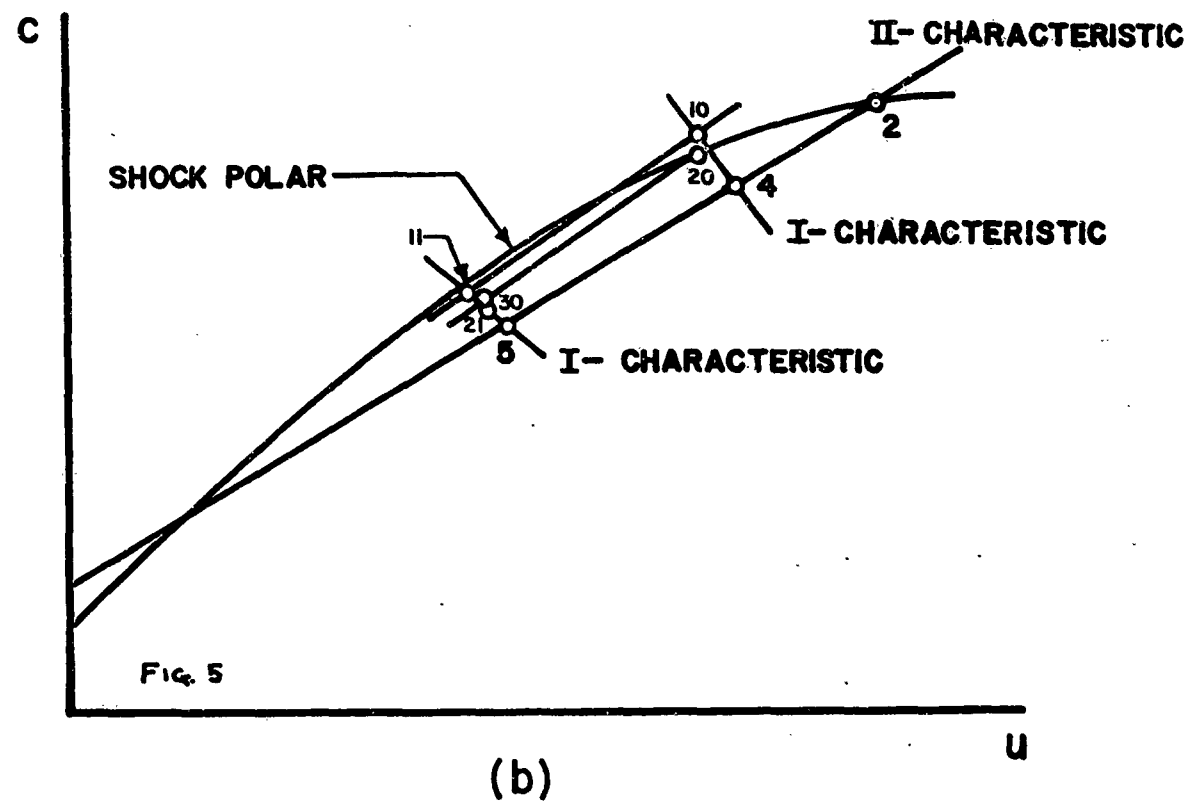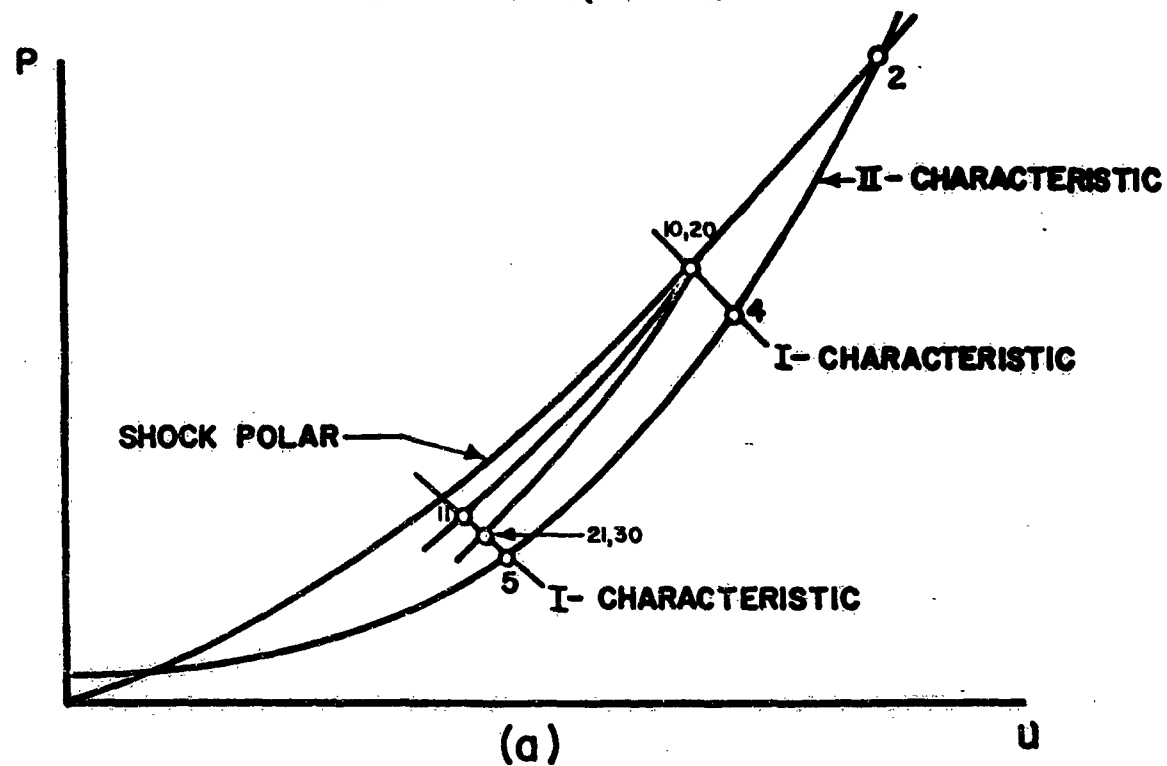
Figure 5.   State Planes for Aluminum (Schematic).
    a.   P,u-State Plane
    b.   c,u-State Plane
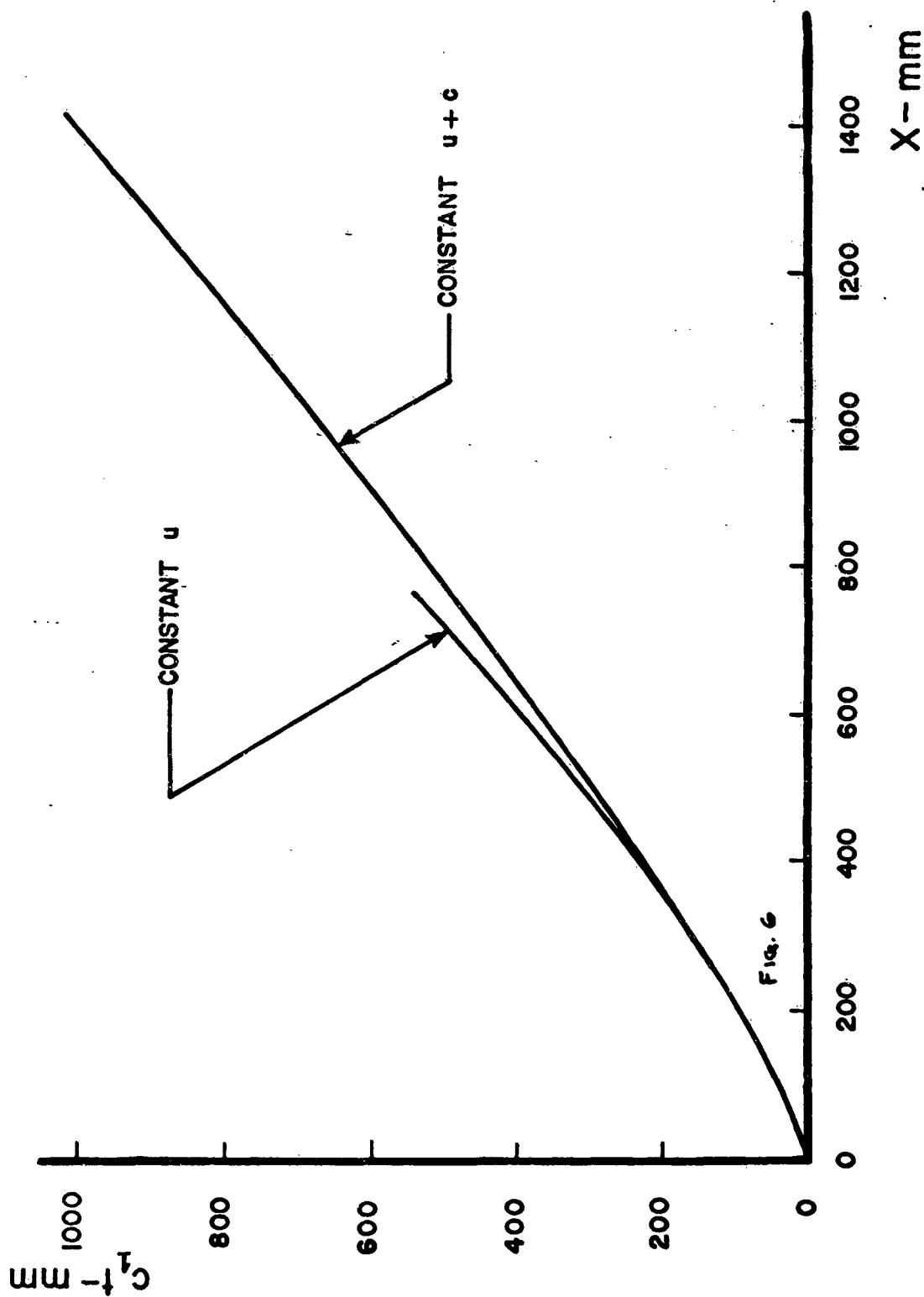
Figure 6. Position of Shock Front by Present Approximations ("constant u + c" and "constant u").
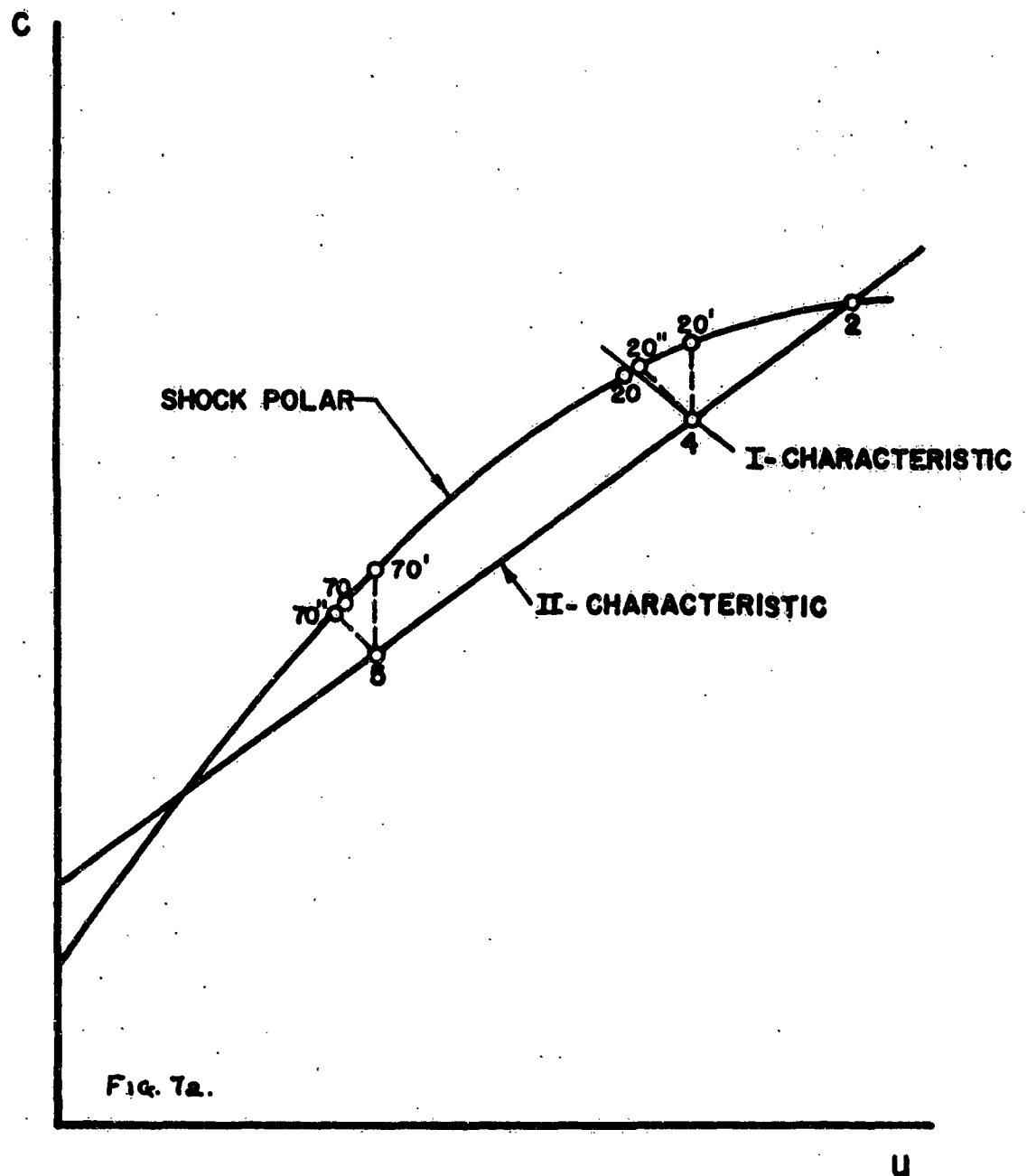
Figure 7a.   Schematic Illustrating the Relative Accuracy of the "constant
u + c" Approach and the "constant u" Approach for Aluminum.
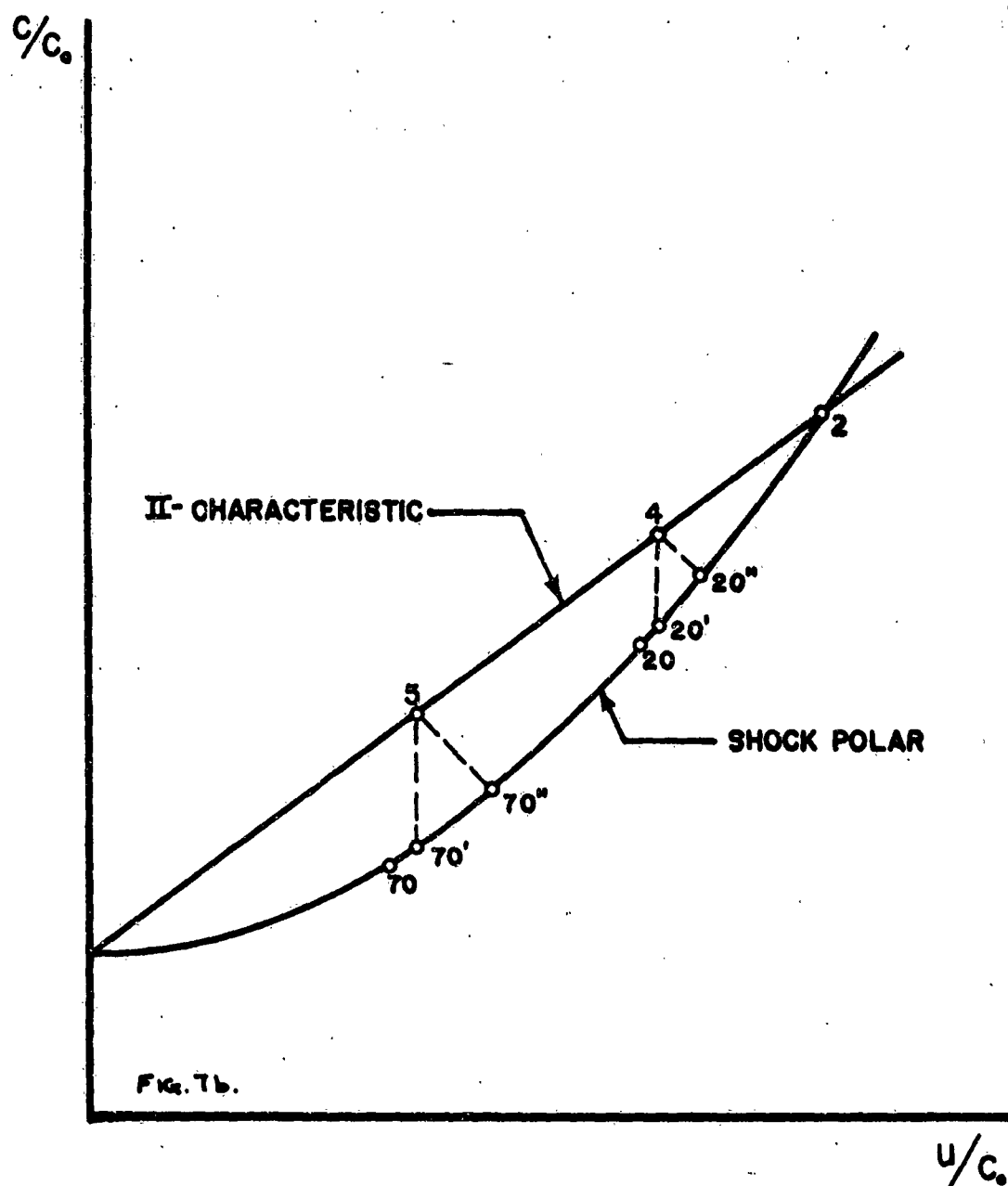
Figure 7b. Schematic Illustrating the Relative Accuracy of the "constant
u + c" Approach and the "constant u" Approach for Ideal Gas.
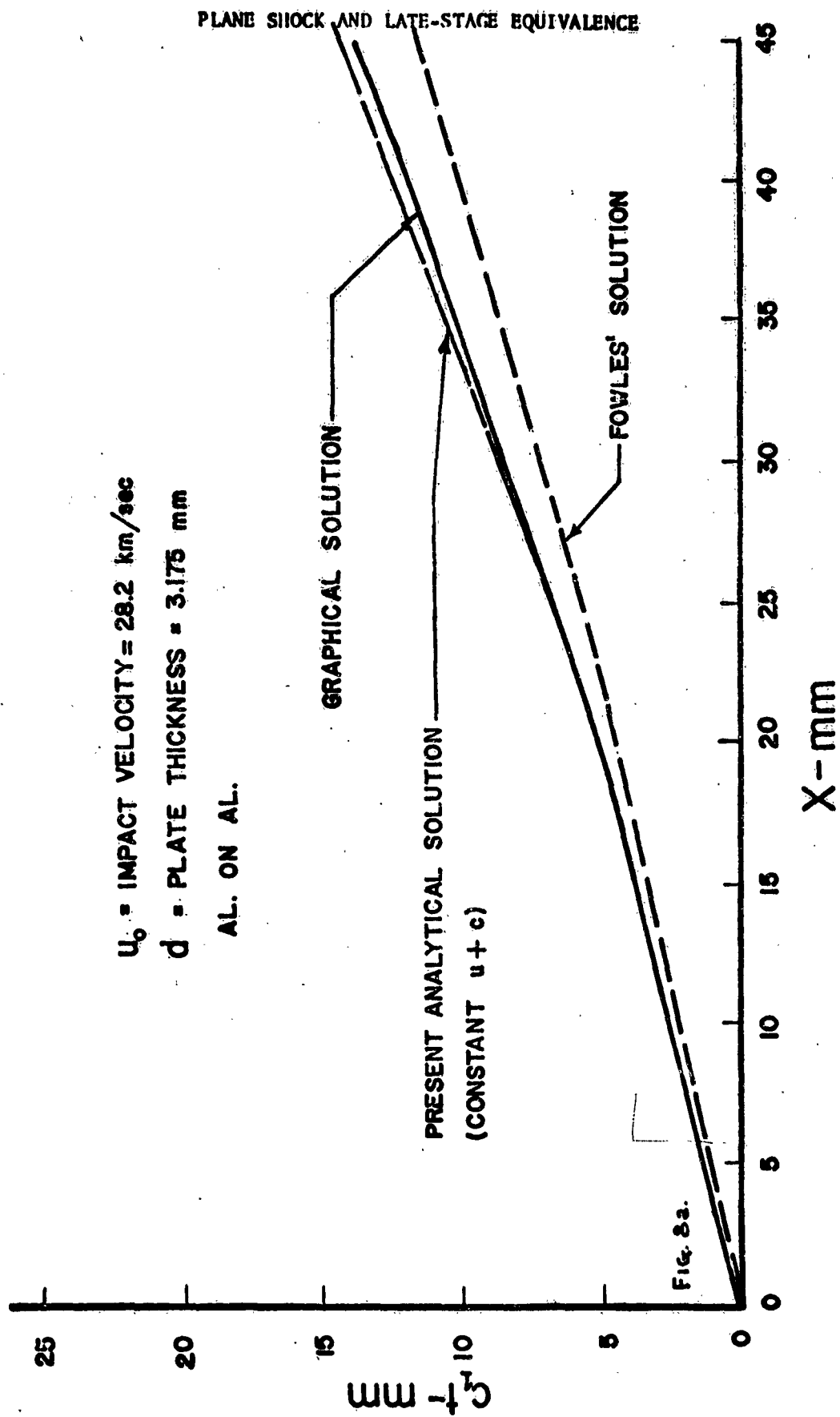
Figure 8a. Position of Shock Front by Different Methods.

53

PLANE SHOCK AND LATE-STAGE EQUIVALENCE

Fig. 8b.
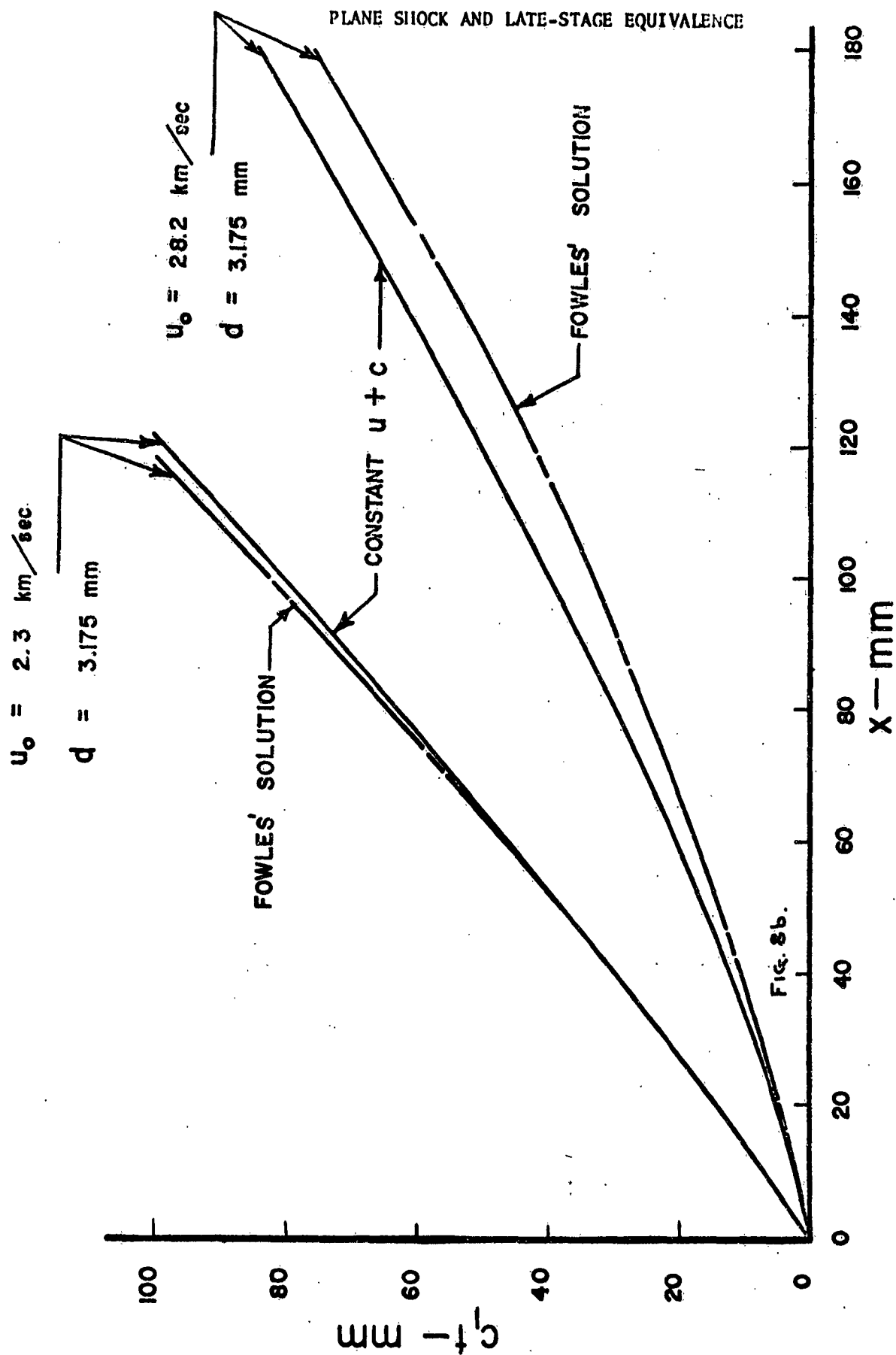
Figure 8b. Comparison of Shock Front by "constant $u + c$" Approach and
Fowles' Solution for Two Impact Velocities.

54
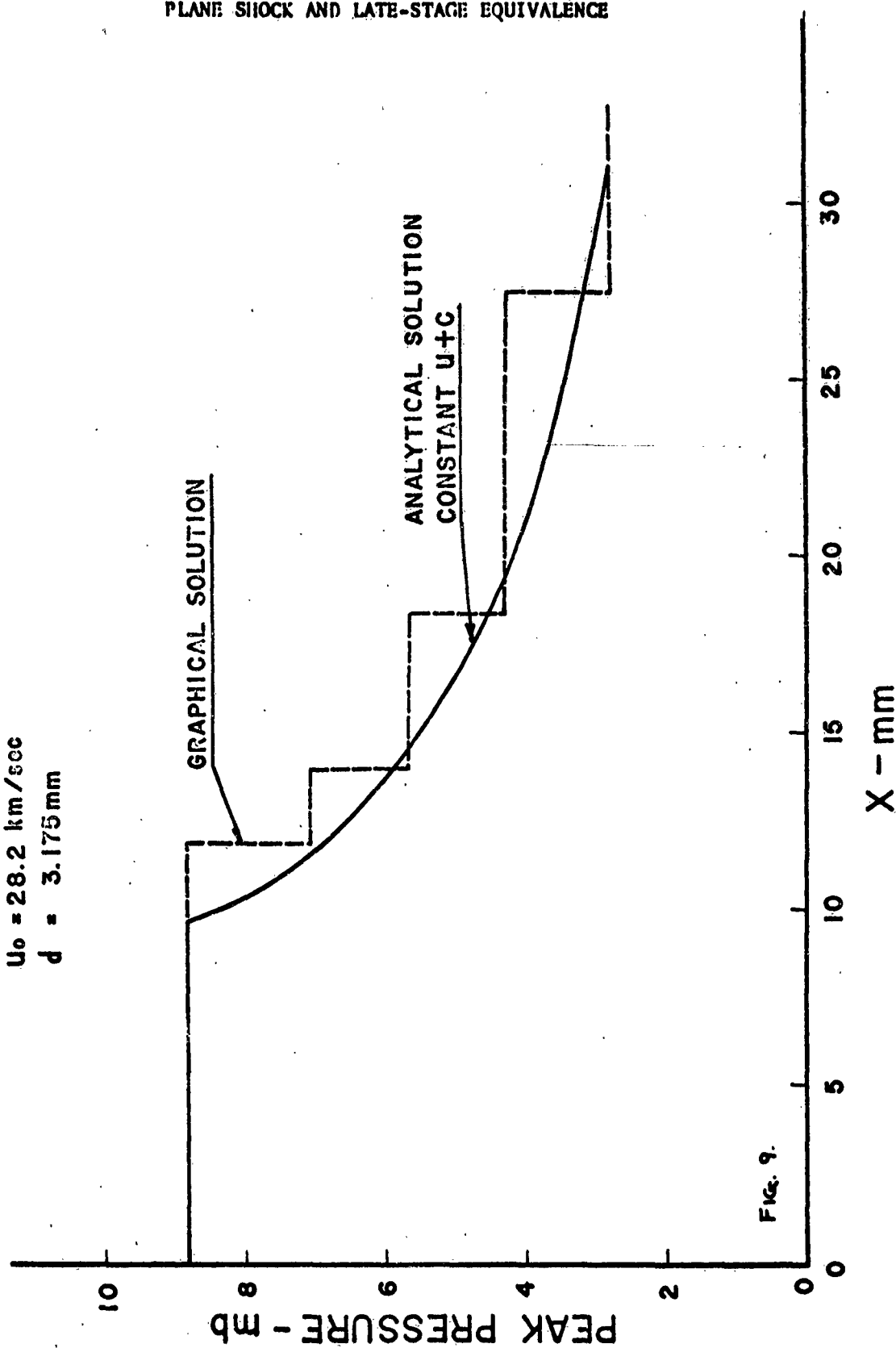
Figure 9. Peak Pressure versus Distance from Point of Impact.

55
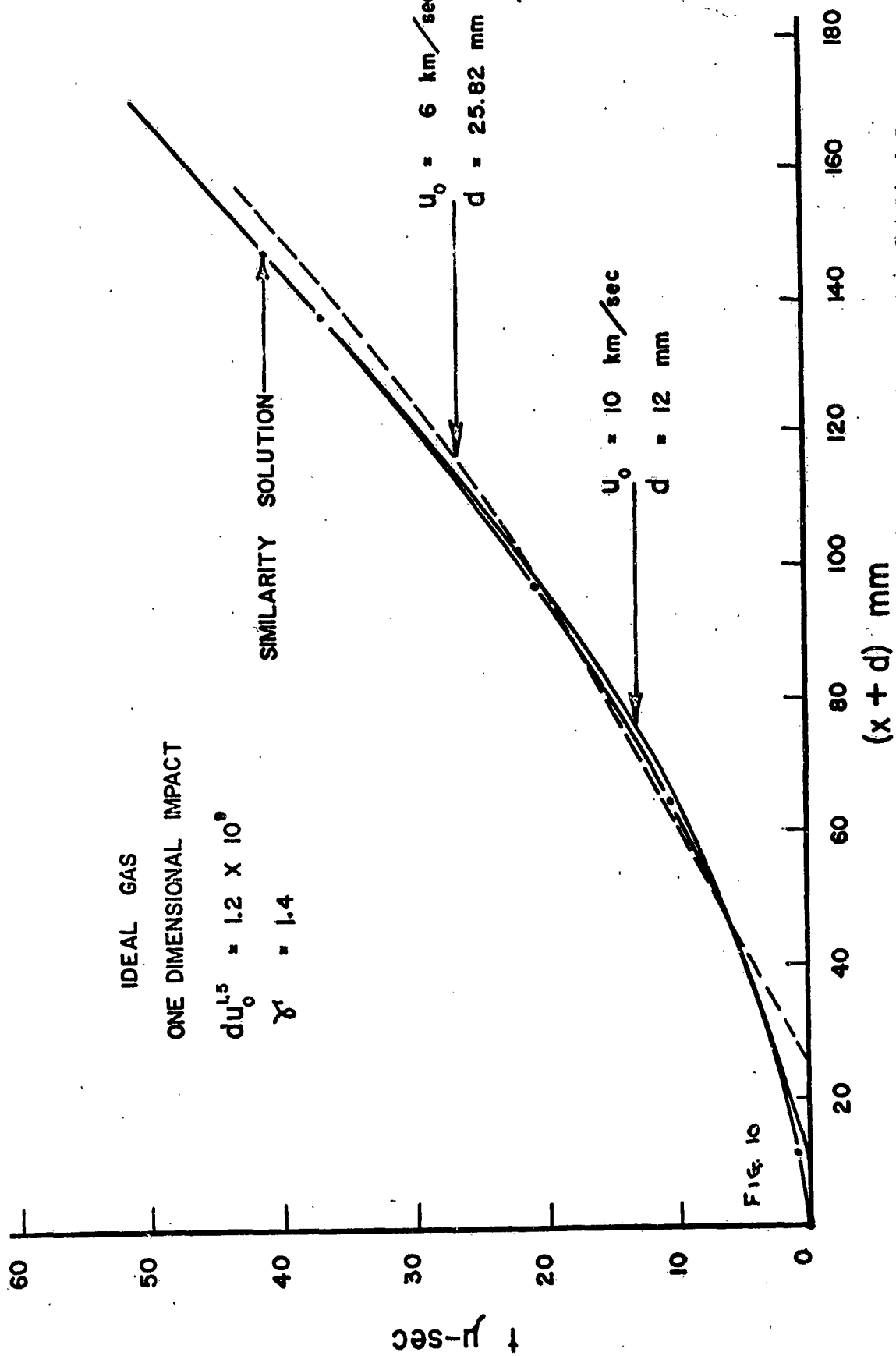
Figure 10. Late-Stage Equivalence Comparison of Time versus Distance from Free Surface for Ideal Gas
(The Similarity Solution is $x + d = 1.5924t^{.6}$)

PLANE SHOCK AND LATE-STAGE EQUIVALENCE

IDEAL GAS

ONE-DIMENSIONAL IMPACT

$du_o^{1.5} = 1.2 \times 10^9 \left(\frac{cm^2}{sec}\right)^{1.5}$

$\gamma = 1.4$

$U_o = 10 \text{ km}/\text{sec}$

$U_o = 9 \text{ km}/\text{sec}$

SIMILARITY SOLUTION

$U_o = 6 \text{ km}/\text{sec}$

$(X + d) \text{ mm}$
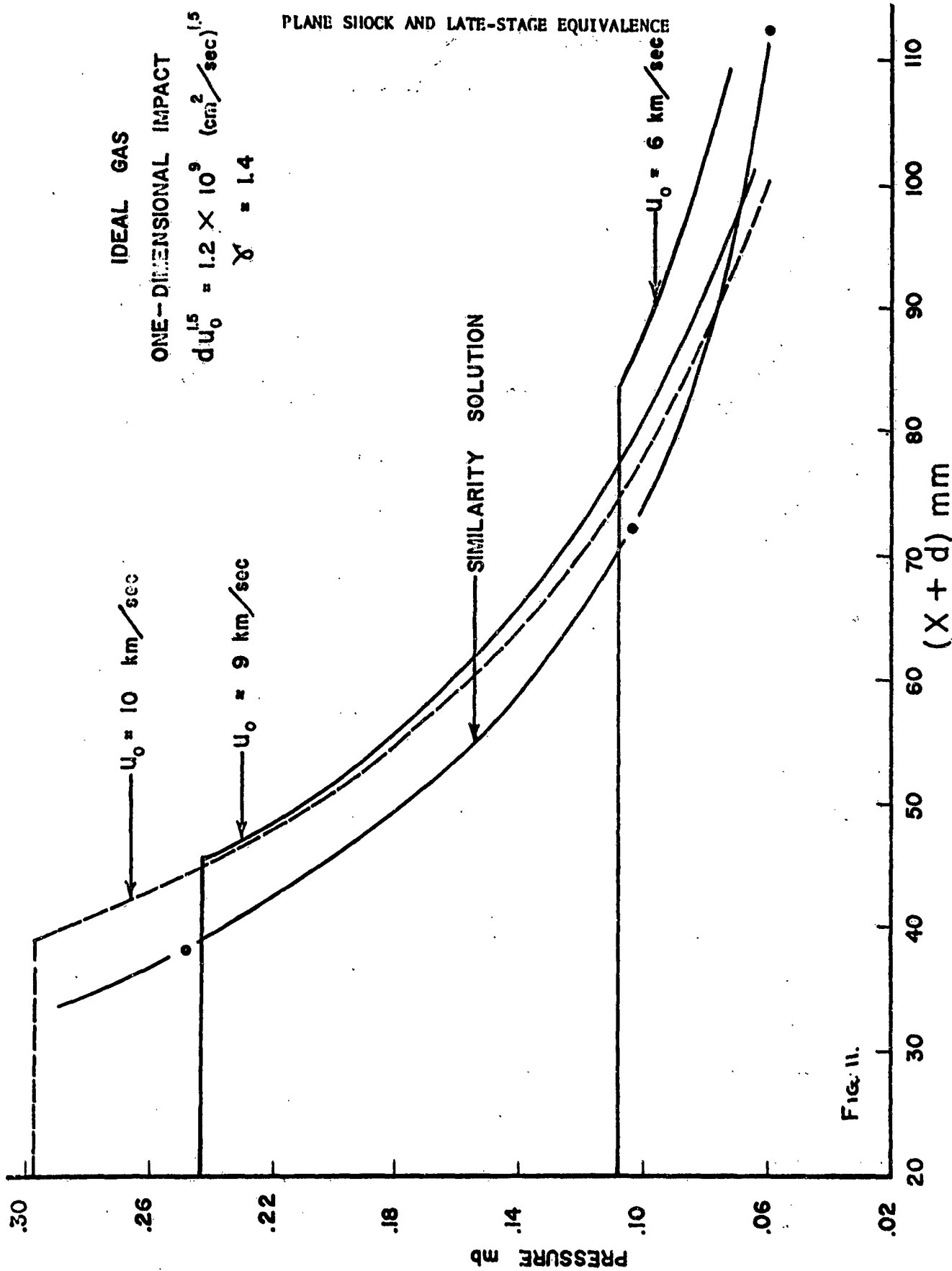
PRESSURE mb

FIG. 11.

Figure 11. Late-Stage Equivalence Comparison of Peak Pressure versus Distance From Free Surface for Ideal Gas. (The Similarity Solution is $x + d = 1.5924 t^{.6}$).
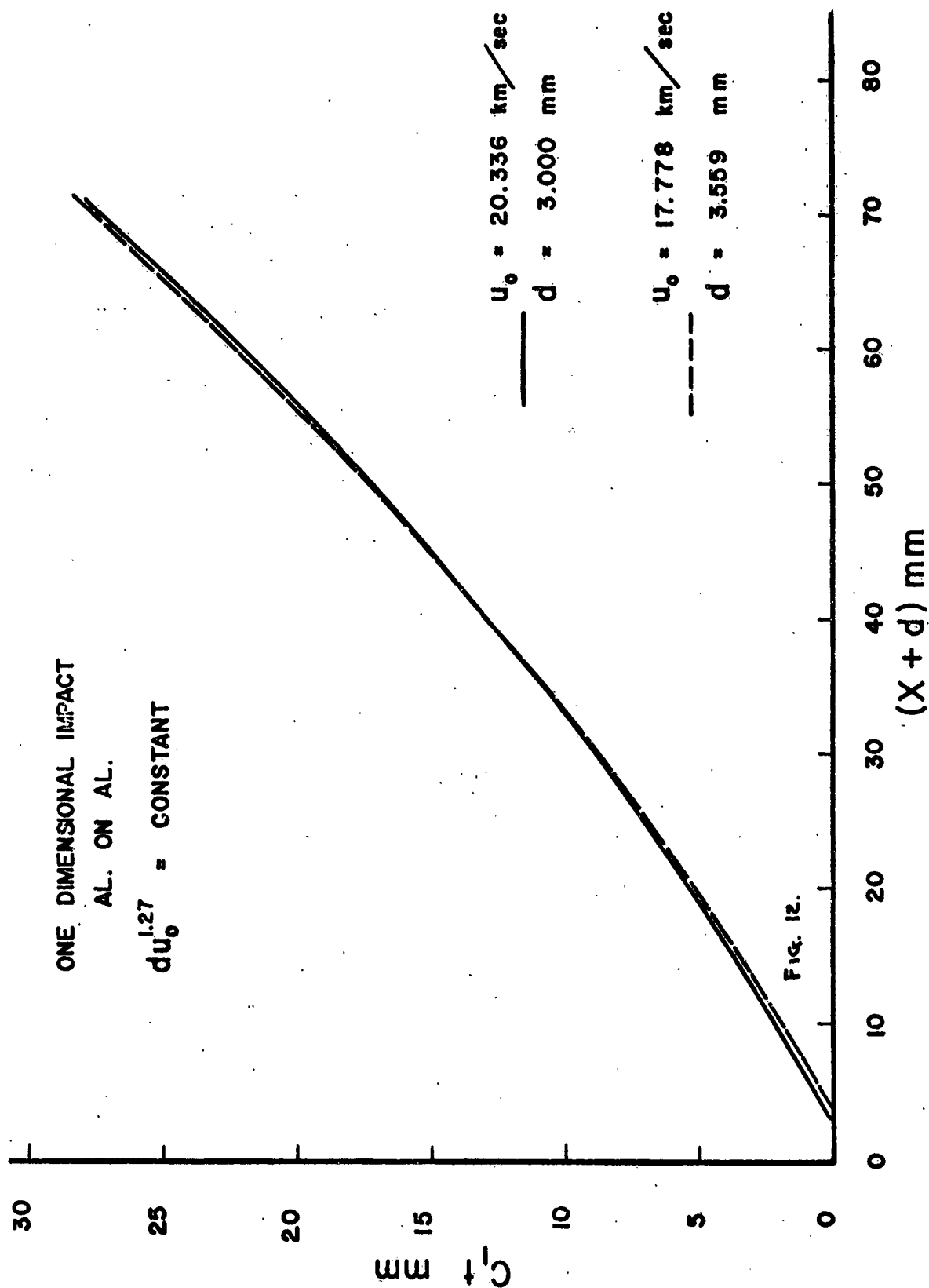
Figure 12. Late-Stage Equivalence Comparison of Time versus Distance from Free Surface (Aluminum).

ONE DIMENSIONAL IMPACT AL. ON AL.

	u_o (km/sec)	d (mm)
A	37.446	.500
B	31.644	.619
C	27.076	.754

$$du_o^{1.27} = \text{CONSTANT}$$

X— mm

PRESSURE mb

FIG. 13a.
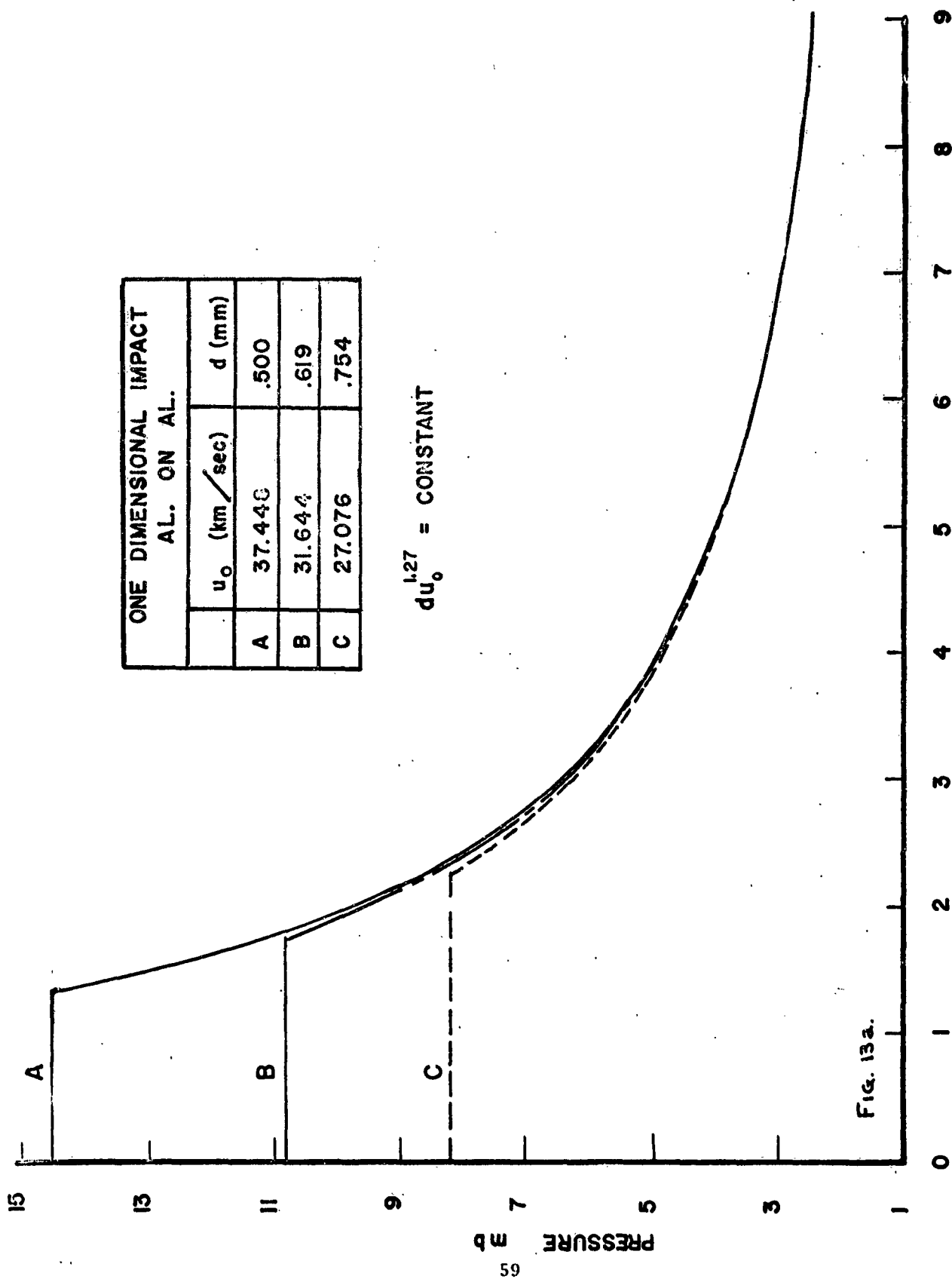
Figure 13a. Late-Stage Equivalence Comparison of Peak Pressure versus Distance from Point of Impact (Aluminum).
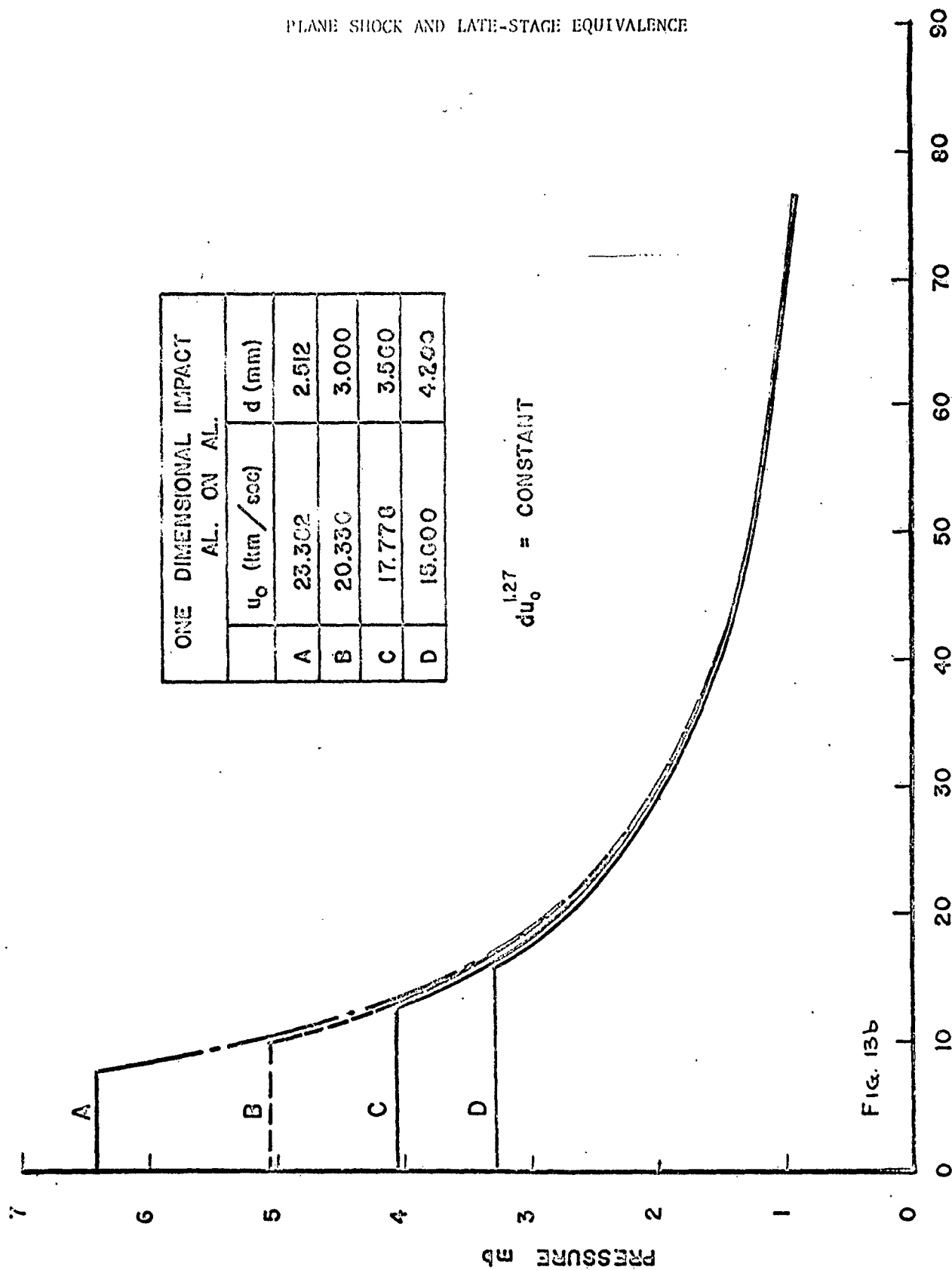
Figure 13b. Late-Stage Equivalence Comparison of Peak Pressure versus Distance from Point of Impact (Aluminum).

ONE DIMENSIONAL IMPACT AL. ON AL.		
	u_o (km/sec)	d (mm)
A	9.394	2.551
B	8.268	3.000
C	7.262	3.537
D	6.358	4.187

$$du_o^{1.27} = \text{CONSTANT}$$

Fig. 13c.

Figure 13c. Late-Stage Equivalence Comparison of Peak Pressure versus Distance from Point of Impact (Aluminum).

PRESSURE mb

X — mm

ONE DIMENSIONAL IMPACT
AL. ON AL.

	u (km sec)	d (mm)
A	4.340	3.000
B	3.664	3.719
C	2.930	4.940

$$d u_o^{1.27} = \text{CONSTANT}$$

PRESSURE - mb

X — mm

Fig. 13d.

Figure 13d. Late-Stage Equivalence Comparison of Peak Pressure versus Distance from Point of Impact (Aluminum).

ONE DIMENSIONAL IMPACT CU ON CU			
	u_o (km/sec)	d (mm)	PEAK PRESSURE
A	22.018	2.098	20.544
B	17.842	3.000	14.166
C	14.504	4.266	9.855
D	11.882	5.988	6.981

$$d u_o^{1.70} = \text{CONSTANT}$$

Fig. 14.

Figure 14. Late-Stage Equivalence Comparison of
Peak Pressure versus Distance from Point of Impact (Copper).

63

Figure 15.   P,u-State Plane
             a. Aluminum
             b. Copper
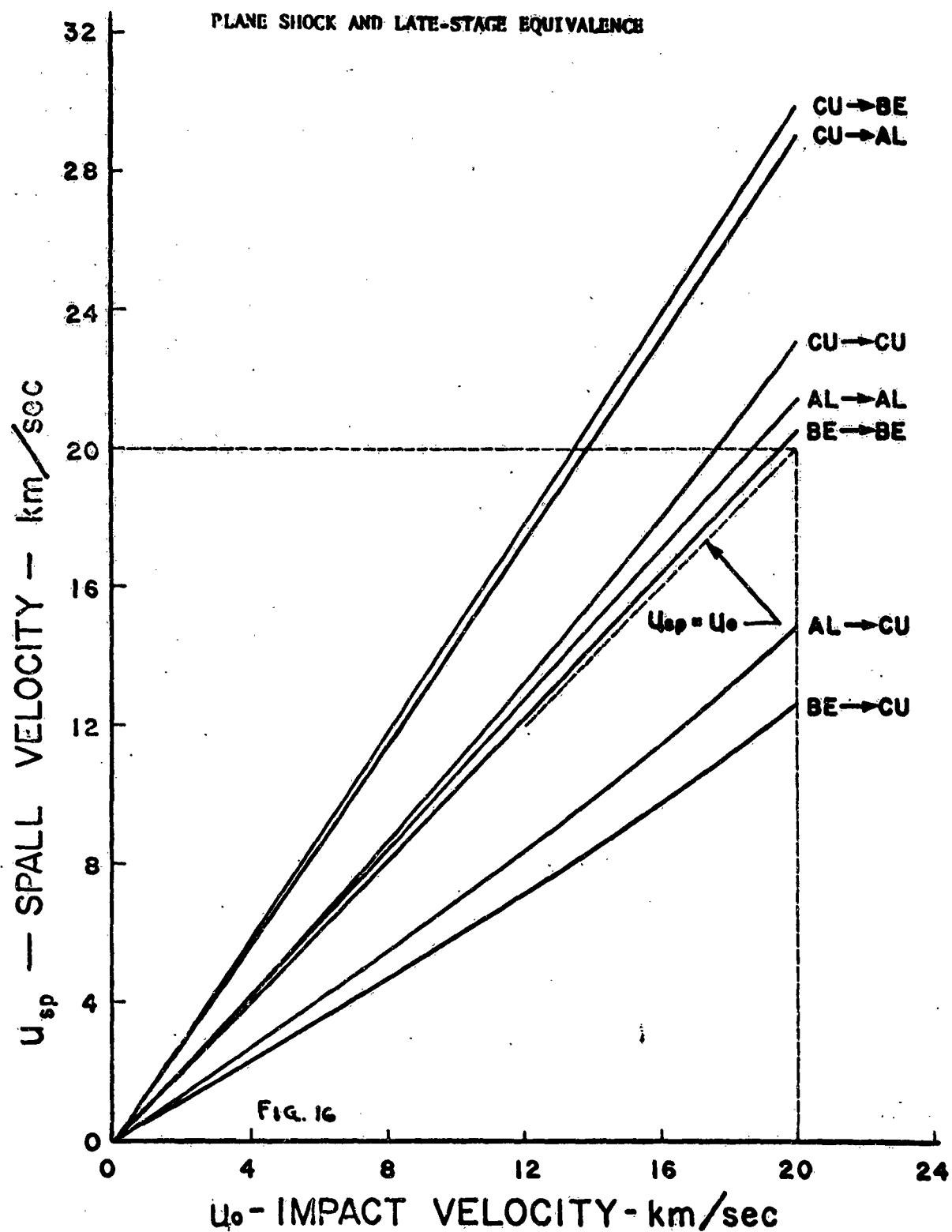
Figure 16.   Spall Velocity of the Target Free Surface Due
to One-Dimensional Impact.
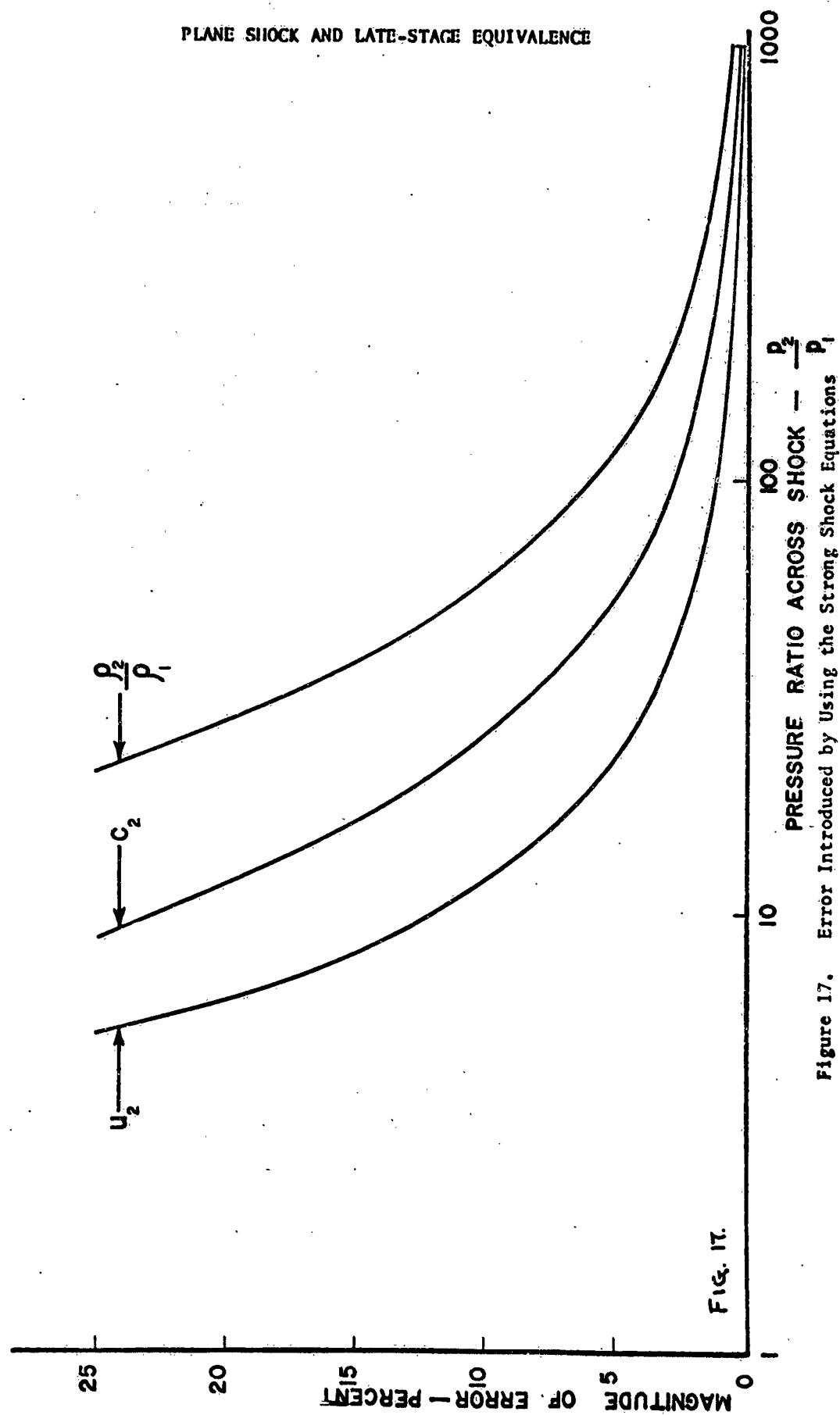
Figure 17. Error Introduced by Using the Strong Shock Equations

FIG. 17.

Table I   Equation of State Data for Aluminum
(For details, see Appendix A)

u	U	P_H	ρ_0/ρ_H	c_H	Z	γ	A'	P_0
.50	6.017	.081	.917	5.89	6.390	4.562	.166	.0006
.55	6.092	.090	.910	5.96	6.510	4.538	.167	.0007
.60	6.166	.100	.903	6.03	6.630	4.513	.168	.0009
.65	6.240	.110	.896	6.09	6.740	4.489	.170	.0011
.70	6.314	.119	.889	6.16	6.860	4.465	.171	.0013
.75	6.388	.129	.883	6.23	6.980	4.441	.172	.0016
.80	6.461	.140	.876	6.30	7.100	4.418	.174	.0019
.85	6.535	.150	.870	6.36	7.210	4.395	.175	.0023
.90	6.608	.161	.864	6.43	7.330	4.372	.176	.0026
.95	6.681	.171	.858	6.50	7.450	4.350	.178	.0030
1.00	6.754	.182	.852	6.57	7.570	4.328	.179	.0035
1.05	6.827	.194	.846	6.64	7.690	4.306	.180	.0039
1.10	6.900	.205	.841	6.70	7.800	4.284	.182	.0044
1.15	6.972	.216	.835	6.77	7.920	4.263	.183	.0050
1.20	7.045	.228	.830	6.84	8.040	4.242	.185	.0055
1.25	7.117	.240	.824	6.91	8.160	4.221	.186	.0061
1.30	7.189	.252	.819	6.98	8.280	4.201	.188	.0067
1.35	7.261	.265	.814	7.04	8.390	4.180	.189	.0074
1.40	7.333	.277	.809	7.11	8.510	4.160	.191	.0081
1.45	7.404	.290	.804	7.18	8.630	4.141	.192	.0088
1.50	7.476	.303	.799	7.25	8.750	4.121	.194	.0095
1.55	7.547	.316	.795	7.32	8.870	4.102	.195	.0103
1.60	7.618	.329	.790	7.38	8.980	4.084	.197	.0111
1.65	7.689	.343	.785	7.45	9.100	4.065	.199	.0120
1.70	7.760	.356	.781	7.52	9.220	4.047	.200	.0128
1.75	7.831	.370	.777	7.59	9.340	4.029	.202	.0137
1.80	7.901	.384	.772	7.66	9.460	4.011	.203	.0147
1.85	7.972	.398	.768	7.73	9.580	3.994	.205	.0156
1.90	8.041	.413	.764	7.81	9.710	3.982	.206	.0166
1.95	8.111	.427	.760	7.87	9.820	3.962	.208	.0177
2.00	8.180	.442	.755	7.94	9.940	3.941	.211	.0188
2.05	8.249	.457	.751	8.01	10.060	3.921	.213	.0199
2.10	8.318	.472	.748	8.07	10.170	3.901	.215	.0211
2.15	8.387	.487	.744	8.14	10.290	3.881	.217	.0223
2.20	8.456	.502	.740	8.21	10.410	3.862	.219	.0235
2.25	8.524	.518	.736	8.27	10.520	3.843	.221	.0248
2.30	8.593	.534	.732	8.34	10.640	3.824	.223	.0260
2.35	8.661	.550	.729	8.40	10.750	3.805	.226	.0273
2.40	8.730	.566	.725	8.47	10.870	3.786	.228	.0286
2.45	8.798	.582	.722	8.53	10.980	3.768	.230	.0299
2.50	8.866	.598	.718	8.60	11.100	3.750	.232	.0312
2.55	8.934	.615	.715	8.66	11.210	3.733	.234	.0326
2.60	9.002	.632	.711	8.73	11.330	3.715	.237	.0340
2.65	9.070	.649	.708	8.79	11.440	3.698	.239	.0354
2.70	9.137	.666	.705	8.86	11.560	3.681	.241	.0368
2.75	9.205	.683	.701	8.92	11.670	3.664	.243	.0383
2.80	9.272	.701	.698	8.98	11.780	3.648	.246	.0397
2.85	9.340	.719	.695	9.04	11.890	3.631	.248	.0412
2.90	9.407	.737	.692	9.11	12.010	3.615	.250	.0427
2.95	9.474	.755	.689	9.17	12.120	3.600	.252	.0443

PLANE SHOCK AND LATE-STAGE EQUIVALENCE

u	U	P_H	ρ_o/ρ_H	c_H	Z	Y	A'	P_o
3.00	9.541	.773	.686	9.23	12.230	3.584	.255	.0458
3.05	9.608	.791	.683	9.29	12.340	3.569	.257	.0474
3.10	9.675	.810	.680	9.35	12.450	3.554	.259	.0490
3.15	9.741	.828	.677	9.42	12.570	3.539	.261	.0506
3.20	9.808	.847	.674	9.48	12.680	3.525	.264	.0522
3.25	9.874	.866	.671	9.54	12.790	3.511	.266	.0539
3.30	9.940	.886	.668	9.60	12.900	3.497	.268	.0556
3.35	10.007	.905	.665	9.66	13.010	3.483	.271	.0573
3.40	10.073	.925	.662	9.72	13.120	3.469	.273	.0590
3.45	10.139	.944	.660	9.78	13.230	3.456	.275	.0608
3.50	10.204	.964	.657	9.84	13.340	3.443	.278	.0625
3.55	10.270	.984	.654	9.90	13.450	3.430	.280	.0643
3.60	10.336	1.005	.652	9.96	13.560	3.418	.282	.0661
3.65	10.401	1.025	.649	10.01	13.660	3.406	.285	.0679
3.70	10.467	1.046	.646	10.07	13.770	3.393	.287	.0698
3.75	10.532	1.066	.644	10.13	13.880	3.382	.289	.0717
3.80	10.597	1.087	.641	10.19	13.990	3.370	.292	.0736
3.85	10.662	1.108	.639	10.25	14.100	3.359	.294	.0755
3.90	10.727	1.130	.636	10.30	14.200	3.348	.297	.0774
3.95	10.792	1.151	.634	10.36	14.310	3.337	.299	.0794
4.00	10.857	1.173	.632	10.42	14.420	3.327	.301	.0813
4.05	10.921	1.194	.629	10.47	14.520	3.316	.304	.0833
4.10	10.986	1.216	.627	10.53	14.630	3.306	.306	.0854
4.15	11.050	1.238	.624	10.59	14.740	3.297	.309	.0874
4.20	11.114	1.260	.622	10.64	14.840	3.287	.311	.0895
4.25	11.179	1.283	.620	10.70	14.950	3.278	.313	.0915
4.30	11.243	1.305	.618	10.75	15.050	3.269	.316	.0936
4.35	11.307	1.328	.615	10.81	15.160	3.260	.318	.0958
4.40	11.370	1.351	.613	10.86	15.260	3.251	.321	.0979
4.45	11.434	1.374	.611	10.92	15.370	3.243	.323	.1001
4.50	11.498	1.397	.609	10.97	15.470	3.235	.326	.1023
4.60	11.614	1.442	.604	11.06	15.660	3.216	.331	.1068
4.70	11.740	1.490	.600	11.16	15.860	3.199	.336	.1111
4.80	11.866	1.538	.595	11.27	16.070	3.183	.341	.1155
4.90	11.992	1.587	.591	11.37	16.270	3.167	.346	.1199
5.00	12.118	1.636	.587	11.47	16.470	3.152	.352	.1244
5.10	12.244	1.686	.583	11.58	16.680	3.136	.357	.1289
5.20	12.370	1.737	.580	11.68	16.880	3.121	.362	.1334
5.30	12.495	1.788	.576	11.78	17.080	3.107	.367	.1380
5.40	12.621	1.840	.572	11.88	17.280	3.092	.372	.1426
5.50	12.746	1.893	.568	11.98	17.480	3.078	.377	.1472
5.60	12.871	1.946	.565	12.08	17.680	3.064	.382	.1519
5.70	12.997	2.000	.561	12.18	17.880	3.050	.387	.1566
5.80	13.122	2.055	.558	12.28	18.080	3.036	.392	.1613
5.90	13.247	2.110	.555	12.38	18.280	3.023	.397	.1661
6.00	13.372	2.166	.551	12.48	18.480	3.010	.403	.1709
6.10	13.497	2.223	.548	12.58	18.680	2.997	.408	.1758
6.20	13.621	2.280	.545	12.67	18.870	2.985	.413	.1807
6.30	13.746	2.338	.542	12.77	19.070	2.972	.418	.1856
6.40	13.871	2.397	.539	12.87	19.270	2.960	.423	.1906
6.50	13.995	2.456	.536	12.96	19.460	2.949	.428	.1956
6.60	14.119	2.516	.533	13.06	19.660	2.937	.434	.2006
6.70	14.244	2.577	.530	13.15	19.850	2.926	.439	.2057

68

PLANE SHOCK AND LATE-STAGE EQUIVALENCE

u	U	P_H	ρ_o/ρ_H	c_{II}	Z	γ	A'	P_o
6.80	14.368	2.638	.527	13.25	20.050	2.915	.444	.2108
6.90	14.492	2.700	.524	13.34	20.240	2.904	.449	.2159
7.00	14.616	2.762	.521	13.44	20.440	2.894	.454	.2211
7.10	14.740	2.826	.518	13.53	20.630	2.883	.460	.2263
7.20	14.864	2.890	.516	13.62	20.820	2.873	.465	.2316
7.30	14.987	2.954	.513	13.71	21.010	2.864	.470	.2368
7.40	15.111	3.019	.510	13.81	21.210	2.854	.475	.2422
7.50	15.234	3.085	.508	13.90	21.400	2.845	.480	.2475
7.60	15.358	3.151	.505	13.99	21.590	2.836	.486	.2529
7.70	15.481	3.219	.503	14.08	21.780	2.827	.491	.2584
7.80	15.604	3.286	.500	14.17	21.970	2.818	.496	.2638
7.90	15.728	3.355	.498	14.26	22.160	2.810	.502	.2693
8.00	15.851	3.424	.495	14.35	22.350	2.802	.507	.2749
8.10	15.973	3.493	.493	14.44	22.540	2.794	.512	.2804
8.20	16.096	3.564	.491	14.52	22.720	2.787	.517	.2860
8.30	16.219	3.635	.488	14.61	22.910	2.780	.523	.2917
8.40	16.342	3.706	.486	14.70	23.100	2.773	.528	.2974
8.50	16.464	3.779	.484	14.79	23.290	2.766	.533	.3031
8.60	16.587	3.851	.482	14.87	23.470	2.760	.539	.3089
8.70	16.709	3.925	.479	14.96	23.660	2.753	.544	.3146
8.80	16.831	3.999	.477	15.04	23.840	2.747	.549	.3205
8.90	16.953	4.074	.475	15.13	24.030	2.742	.555	.3263
9.00	17.076	4.149	.473	15.21	24.210	2.736	.560	.3322
9.10	17.197	4.225	.471	15.30	24.400	2.731	.565	.3382
9.20	17.319	4.302	.469	15.38	24.580	2.726	.571	.3441
9.30	17.441	4.379	.467	15.46	24.760	2.721	.576	.3502
9.40	17.563	4.457	.465	15.55	24.950	2.717	.581	.3562
9.50	17.684	4.536	.463	15.63	25.130	2.712	.587	.3623
9.60	17.806	4.615	.461	15.71	25.310	2.708	.592	.3684
9.80	18.036	4.772	.457	15.83	25.630	2.703	.602	.3802
10.00	18.278	4.935	.453	15.98	25.980	2.693	.613	.3926
10.20	18.520	5.100	.449	16.13	26.330	2.684	.623	.4052
10.40	18.761	5.268	.446	16.29	26.690	2.674	.634	.4180
10.60	19.003	5.439	.442	16.44	27.040	2.665	.645	.4312
10.80	19.245	5.612	.439	16.59	27.390	2.656	.656	.4445
11.00	19.486	5.787	.435	16.74	27.740	2.647	.667	.4581
11.20	19.728	5.966	.432	16.89	28.090	2.637	.678	.4719
11.40	19.969	6.147	.429	17.04	28.440	2.628	.690	.4860
11.60	20.211	6.330	.426	17.19	28.790	2.620	.701	.5003
11.80	20.452	6.516	.423	17.34	29.140	2.611	.713	.5148
12.00	20.694	6.705	.420	17.49	29.490	2.602	.725	.5296
12.20	20.936	6.896	.417	17.64	29.840	2.593	.737	.5447
12.40	21.177	7.090	.414	17.79	30.190	2.585	.749	.5600
12.60	21.419	7.287	.412	17.94	30.540	2.576	.762	.5755
12.80	21.660	7.486	.409	18.09	30.890	2.568	.775	.5912
13.00	21.901	7.687	.406	18.23	31.230	2.560	.787	.6072
13.20	22.143	7.892	.404	18.38	31.580	2.552	.800	.6235
13.40	22.384	8.099	.401	18.53	31.930	2.544	.814	.6400
13.60	22.626	8.308	.399	18.67	32.270	2.535	.827	.6567
13.80	22.867	8.520	.397	18.82	32.620	2.528	.840	.6737
14.00	23.109	8.735	.394	18.97	32.970	2.520	.854	.6909
14.20	23.350	8.952	.392	19.11	33.310	2.512	.868	.7083
14.40	23.591	9.172	.390	19.26	33.660	2.504	.882	.7260

PLANE SHOCK AND LATE-STAGE EQUIVALENCE

u	U	P_H	ρ_o/ρ_H	c_H	Z	γ	A'	P_o
14.60	23.833	9.395	.387	19.40	34.000	2.497	.896	.7440
14.80	24.074	9.620	.385	19.54	34.340	2.489	.910	.7622
15.00	24.315	9.848	.383	19.69	34.690	2.482	.925	.7806
15.20	24.557	10.078	.381	19.83	35.030	2.474	.940	.7993
15.40	24.798	10.311	.379	19.97	35.370	2.467	.954	.8182
15.60	25.039	10.547	.377	20.12	35.720	2.460	.969	.8373
15.80	25.280	10.785	.375	20.26	36.060	2.453	.984	.8567
16.00	25.522	11.025	.373	20.40	36.400	2.446	1.000	.8763
16.20	25.763	11.269	.371	20.54	36.740	2.439	1.015	.8962
16.40	26.004	11.515	.369	20.68	37.080	2.432	1.031	.9163
16.60	26.245	11.763	.368	20.83	37.430	2.425	1.047	.9367
16.80	26.487	12.014	.366	20.97	37.770	2.419	1.063	.9573
17.00	26.728	12.268	.364	21.11	38.110	2.412	1.079	.9781
17.20	26.969	12.524	.362	21.25	38.450	2.405	1.095	.9992
17.40	27.210	12.783	.361	21.38	38.780	2.399	1.112	1.0206
17.60	27.451	13.045	.359	21.52	39.120	2.393	1.128	1.0421
17.80	27.692	13.309	.357	21.66	39.460	2.386	1.145	1.0639
18.00	27.933	13.576	.356	21.80	39.800	2.380	1.162	1.0860
18.20	28.174	13.845	.354	21.94	40.140	2.374	1.179	1.1083
18.40	28.415	14.117	.352	22.08	40.480	2.368	1.197	1.1308
18.60	28.657	14.391	.351	22.21	40.810	2.362	1.214	1.1536
18.80	28.898	14.668	.349	22.35	41.150	2.357	1.232	1.1766
19.00	29.139	14.948	.348	22.48	41.480	2.351	1.250	1.1999
19.20	29.380	15.230	.346	22.62	41.820	2.345	1.268	1.2234
19.40	29.621	15.515	.345	22.76	42.160	2.340	1.286	1.2471
19.60	29.862	15.803	.344	22.89	42.490	2.334	1.304	1.2711
19.80	30.103	16.093	.342	23.03	42.830	2.329	1.323	1.2953
20.00	30.343	16.385	.341	23.16	43.160	2.323	1.342	1.3198
20.20	30.584	16.681	.340	23.29	43.490	2.318	1.360	1.3445
20.40	30.825	16.979	.338	23.43	43.830	2.313	1.379	1.3695
20.60	31.066	17.279	.337	23.56	44.160	2.308	1.399	1.3947
20.80	31.307	17.582	.336	23.69	44.490	2.303	1.418	1.4201
21.00	31.548	17.888	.334	23.83	44.830	2.298	1.437	1.4458
21.20	31.789	18.196	.333	23.96	45.160	2.293	1.457	1.4717
21.40	32.030	18.507	.332	24.09	45.490	2.289	1.477	1.4979
21.60	32.271	18.820	.331	24.22	45.820	2.284	1.497	1.5243
21.80	32.511	19.136	.329	24.35	46.150	2.279	1.517	1.5509
22.00	32.752	19.455	.328	24.48	46.480	2.275	1.537	1.5778
22.20	32.993	19.776	.327	24.61	46.810	2.271	1.558	1.6050
22.40	33.234	20.100	.326	24.74	47.140	2.266	1.579	1.6323
22.60	33.474	20.426	.325	24.87	47.470	2.262	1.600	1.6600
22.80	33.715	20.755	.324	25.00	47.800	2.258	1.621	1.6878
23.00	33.956	21.087	.323	25.13	48.130	2.254	1.642	1.7159
23.20	34.197	21.421	.322	25.26	48.460	2.250	1.663	1.7443
23.40	34.437	21.758	.321	25.39	48.790	2.246	1.685	1.7728
23.60	34.678	22.097	.319	25.52	49.120	2.242	1.706	1.8017
23.80	34.919	22.439	.318	25.64	49.440	2.239	1.728	1.8307
24.00	35.159	22.783	.317	25.77	49.770	2.235	1.750	1.8601
24.20	35.400	23.130	.316	25.90	50.100	2.232	1.772	1.8896
24.40	35.641	23.480	.315	26.02	50.420	2.228	1.795	1.9194
24.60	35.881	23.832	.314	26.15	50.750	2.225	1.817	1.9494
24.80	36.122	24.187	.313	26.27	51.070	2.221	1.840	1.9797
25.00	36.362	24.545	.312	26.40	51.400	2.218	1.863	2.0102

PLANE SHOCK AND LATE-STAGE EQUIVALENCE

REGION	km/sec	km/sec	megabars
	u	c	p
1	0	5.27	0
2	14.10	18.08	8.84
3	0	7.50	.30
4	12.50	16.88	6.96
5	11.00	15.76	5.52
6	9.00	14.26	3.92
7	7.00	12.76	2.65
8	5.00	11.27	1.64
9	2.50	9.40	0.85
10	12.38	16.97	7.06
11	10.87	15.84	5.62
12	8.88	14.34	4.00
20	12.38	16.96	7.06
21	10.94	15.81	5.57
22	8.93	14.31	3.97
30	10.94	15.81	5.57
31	8.98	14.25	3.93
32	8.98	14.27	3.93
50	10.85	15.88	5.65
51	8.90	14.31	4.01
70	10.85	15.92	5.65
71	8.96	14.27	3.95
90	8.96	14.36	3.95
120	8.85	14.48	4.03
130	7.04	14.40	2.68
140	6.98	13.05	2.75

TABLE 2 — PARTIAL LIST OF STATE PROPERTIES

(Regions Correspond to those shown in Figure 4)

Initial Data:

Aluminum on Aluminum Impact

u_o = impact velocity = 28.2 km/sec.

$u_1 = o$, $P_1 = o$, $c_1 = 5.275$ km/sec.

d= 3.175 mm.

PLANE SHOCK AND LATE-STAGE EQUIVALENCE

REGIONS COMPARED		Properties within simple wave		Properties behind shock		change in u $\dfrac{u_H - u}{u}$	change in c $\dfrac{c_H - c}{c}$	change in u + c $\dfrac{(u+c)_H - (u+c)}{(u+c)}$
Region in simple wave (no subscript)	Region behind shock (subscript H)	u (km/sec)	c (km/sec)	u_H (km/sec)	c_H (km/sec)			
4	20	12.5	16.88	12.38	16.97	-.960%	.533%	-.103%
5	70	11.0	15.76	10.86	15.92	-1.270%	1.030%	.070%
6	120	9.0	14.26	8.85	14.48	-1.670%	1.540%	.300%

TABLE 3a

Percent change of u, c, and u + c along a charateristic , according
to the graphical solution (for aluminum with u_o = 28.2 km/sec. d= 3.175 mm.)

72

REGIONS COMPARED		Properties within simple wave		Properties behind shock		change in u $\dfrac{u_H - u}{u}$	change in c $\dfrac{c_H - c}{c}$	change in u + c $\dfrac{(u+c)_H - (u+c)}{(u+c)}$
Region in simple wave (no subscript)	Region behind shock (subscript H)	u (km/sec)	c (km/sec)	u_H (km/sec)	c_H (km/sec)			
4	20	.516	.488	.510	.472	- 1.16%	- 3.28%	- 2.19%
5	70	.430	.470	.423	.445	- 1.63%	- 5.32%	- 3.56%
6	120	.344	.453	.338	.420	- 1.74%	- 7.28%	- 4.89%

TABLE 3b.

Percent change of u, c, and u + c along a characteristic , according to the graphical solution (for an ideal gas with impact velocity of 1.22 km/sec, d= 3.175 mm, c_1 = .344 km/sec, γ = 1.4)

PLANE SHOCK AND LATE-STAGE EQUIVALENCE

APPENDIX A

Equation of State Calculations

In this appendix, the detailed procedure used in computing the properties from the equation of state is outlined. The basic equations involved are those given in Sections III and IV.

Table I[*] contains the equation of state data for aluminum calculated from equation 16,

$$P = \left[a + \frac{b}{\frac{E}{E_o \eta^2} + 1} \right] \frac{E}{V} + A\mu + B\mu^2 \qquad (16)$$

where values for the constants, as determined in Ref. 6, are

a = .5	A = .752 Mb.
b = 1.63	B = .65 Mb.

E_o = .05 (mb - cm^3)/gm.

The first six columns of this table, which correspond to properties on the shock Hugoniot, are calculated from the normal shock conditions, eqs. (1) to (3) and eq. (16), with u_x = 0 and with the subscript "y" dropped. In this table, u is the particle velocity behind the shock, U the shock velocity P_H pressure, ρ_o/ρ_H the density ratio, Z is u + c_H, and c_H is the velocity of sound. All velocities have the units of km/sec, and pressures have the units of megabars.

*This Table replaces Table 1 in D.I.T. #125-5, Ref. 14 which involves a slight error in numerical integration.

74

PLANE SHOCK AND LATE-STAGE EQUIVALENCE

The sound velocity c_H can be obtained either by numerically differentiating the data from eqs. (16) and (9), or it can be obtained from equation (12). The results from eqs. (16) and (9) are shown in Table I.

The isentropes are obtained by numerically integrating eq. (16) with $E = \int - PdV$. These data are not shown in Table I. (The data for a few isentropes are tabulated in Ref. 6 for several metals.) These isentrope data are, instead, fitted to the equation

$$P = A'\left[\left(\frac{\rho}{\rho_o}\right)^{\gamma} - 1\right] + P_o \qquad (11)$$

with a separate set of values of A', γ, and P_o for each isentrope. These values are shown in the last three columns of Table I.

The approximate Hugoniot eqs. (17) and (18) when fitted to the data in Table I have the following form

$$U = 1.9016 + .5947Z + .00145Z^2 \qquad (17)$$

$$U = 5.9179 + 1.2400u - .00081u^2 \qquad (18)$$

In the low pressure region, $P \leq 1$ mb, more accurate data for the shock Hugoniot are available and can be used for the determination of the constants in eqs. (17) and (18). If the low pressure data in Ref. 20, for aluminum, are used, we have

$$U = 2.532 + .45Z + .01Z^2 \qquad (17)$$

$$U = 5.369 + 1.344u - .00156u^2 \qquad (18)$$

75

PLANE SHOCK AND LATE-STAGE EQUIVALENCE

APPENDIX B

One-dimensional Impact in an Ideal Gas

In this appendix, the equations which are used for the study of late-stage equivalence in one-dimensional impacts of ideal gases are derived. The accuracy of the approximate strong shock conditions used in the similarity solutions is also discussed.

For an ideal gas, the equations of state are

$$P = \rho R T$$
$$E = c_v T \tag{B.1}$$
$$c_p - c_v = R$$
$$\gamma = c_p / c_v$$

where T is the absolute temperature and R the gas constant. Combining eqs.(B.1) with the normal shock eqs. (1), (2), and (3), and considering only a right-traveling shock with the stationary region ahead of the shock represented by subscript 1 and the region behind the shock by 2, we have (see Ref. 17, page 1001)

PLANE SHOCK AND LATE-STAGE EQUIVALENCE

$$\frac{u_2}{c_1} = \frac{2}{\gamma+1}\left(\frac{U}{c_1} - \frac{c_1}{U}\right) \qquad (B.2)$$

$$\left(\frac{c_2}{c_1}\right)^2 = 1 + \frac{2(\gamma-1)}{(\gamma+1)^2}\left[\gamma\left(\frac{U}{c_1}\right)^2 - \left(\frac{c_1}{U}\right)^2 - (\gamma-1)\right] \qquad (B.3)$$

$$\frac{\rho_2}{\rho_1} = \frac{1}{1 - \frac{2}{\gamma+1}\left[1 - \left(\frac{c_1}{U}\right)^2\right]} \qquad (B.4)$$

$$\frac{P_2}{P_1} = 1 + \frac{2\gamma}{\gamma+1}\left[\left(\frac{U}{c_1}\right)^2 - 1\right] \qquad (B.5)$$

where $U/c_1 = M_1$ is the Mach number of the shock front with respect to the region ahead. These are the exact shock equations, applicable to strong as well as weak shocks. These shock conditions are too complicated to be used for similarity solutions. For simplification purposes, it is usually necessary to restrict the equations to the case of very strong shocks, i.e., $P_2/P_1 \gg 1$. Under this restriction, eqs. (B.2) to (B.4) reduce to

$$U = \frac{\gamma+1}{2}\, u_2 \qquad (B.6)$$

$$\frac{P_2}{P_1} = \frac{2\gamma}{\gamma+1}\left(\frac{U}{c_1}\right)^2 \text{ or, } P_2 = \frac{2\rho_1}{\gamma+1}\, U^2 \qquad (B.7)$$

77

PLANE SHOCK AND LATE-STAGE EQUIVALENCE

$$c_2^2 = \frac{2\gamma(\gamma-1)}{(\gamma+1)^2} U^2 \qquad\qquad (B.8)$$

$$\frac{\rho_2}{\rho_1} = \frac{\gamma+1}{\gamma-1} \quad (= 6 \text{ for } \gamma = 1.4) \quad (B.9)$$

The condition of $P_2/P_1 = \infty$ is equivalent to $P_1 = E_1 = T_1 = c_1 = 0$, but $\rho_1 \neq 0$. The error involved in using eqs. (B.6) to (B.9) for finite pressure ratios can be calculated directly by comparing these eqs. with the exact equations (B.2) to (B.4). Figure 17 shows the percent error in ρ_2/ρ_1, c_2, and u_2 as functions of P_2/P_1. It can be seen that the maximum error is about 6% at a pressure ratio of 100. This is in agreement with Sedov's[21] results. Taylor's[22] comment that the strong shock equation can be used for pressure ratios above 10 seems to be quite optimistic. Only for pressure ratios above 1000, can we be sure that the maximum error is below one percent. Fortunately, in studying the one-dimensional similarity solution, the main purpose is to formulate an analytical model for the establishment of rules of late-stage equivalence. Thus, the assumption of $P_1 = 0$ (or $E_1 = 0$) is equivalent to $P_2/P_1 = \infty$, and equations (B.6) and (B.9) become exact.

78

PLANE SHOCK AND LATE-STAGE EQUIVALENCE

The isentrope for an ideal gas, obtained from equations
(B.1) and (9), is the familiar isentropic P-ρ relation

$$\frac{P}{\rho^\gamma} = CONSTANT. \qquad (B.10)$$

In solving the impact problem for an ideal gas, the "constant
u" approach is used, since, as previously shown, it is more
accurate than the "constant u + c" approach. The general
equations of state in the form of the Hugoniot eq. (18) and
isentrope eq. (11) are thus replaced by eq. (B.6) and (B.10),
respectively. Notice that the region designated by subscript
2 in eqs. (B.2) to (B.9) represents any region behind the shock
front, e.g., this region is not restricted to region 2 in
Figures 1 and 4.

Due to the simplified form of these two equations, the
initial shock configuration can be expressed explicitly in
terms of u_o, d, and γ. Eqs. (27) and (28), with $t_o = 0$,
$x_o = 0$, become

$$t_1 = \frac{4d}{(\gamma+1)u_o} \qquad (B.11)$$

$$x_1 = \frac{3-\gamma}{\gamma+1} d . \qquad (B.12)$$

79

PLANE SHOCK AND LATE-STAGE EQUIVALENCE

Equations (33) and (34) are replaced by

$$t_3 = \frac{x_1 - \frac{1}{2} u_o \left(1 + \sqrt{\frac{\gamma(\gamma-1)}{2}} \right) t_1}{u_o \left[\frac{\gamma-1}{4} - \frac{1}{2} \sqrt{\frac{\gamma(\gamma-1)}{2}} \right]} \tag{B.13}$$

$$x_3 = \left\{ \frac{x_1 - \frac{1}{2} u_o \left(1 + \sqrt{\frac{\gamma(\gamma-1)}{2}} \right) t_1}{\left[\frac{\gamma-1}{4} - \frac{1}{2} \sqrt{\frac{\gamma(\gamma-1)}{2}} \right]} \right\} \frac{\gamma+1}{4} \,. \tag{B.14}$$

Equation (46) is simplified to

$$\frac{2}{\gamma+1} \frac{dt}{t-t_1} = \frac{du}{\left[\frac{\gamma-1}{4} - \sqrt{\frac{\gamma(\gamma-1)}{8}} \right] u_o} \,. \tag{B.15}$$

After integrating this equation and simplifying, we obtain

a single equation for the shock front

$$x - x_1 = \frac{1}{2} u_o \left\{ 1 + \sqrt{\frac{\gamma(\gamma-1)}{2}} + \left(\frac{\gamma-1}{2} - \sqrt{\frac{\gamma(\gamma-1)}{2}} \right) \ln \left| \frac{t-t_1}{t_3-t_1} \right| \right\} (t - t_1) \,. \tag{B.16}$$

By differentiating (B.16) with respect to t, we obtain the

shock velocity U

$$U = \frac{dx}{dt} = \frac{u_o}{2} \left[\frac{\gamma-1}{2} - \sqrt{\frac{\gamma(\gamma-1)}{2}} \right] + \frac{x - x_1}{t - t_1} \,. \tag{B.17}$$

80

PLANE SHOCK AND LATE-STAGE EQUIVALENCE

APPENDIX C

Spall Velocity Calculation

Equations (19) to (26) are for like-material impacts. In calculating the spall velocity for different-material impacts, these equations must be modified. Using subscript "A" for the target variables and subscript "B" for the projectile variables, we obtain the modified versions of eqs. (19) to (22) as follows

$$\rho_{1A} U_t = \rho_{2A}(U_t - u_{2A}) \left.\right\rbrace \quad \text{TARGET} \qquad (C.1)$$

$$P_{2A} - P_{1A} = \rho_{1A}(U_t u_{2A}) \qquad (C.2)$$

$$\rho_{oB}(U_p - u_o) = \rho_{2B}(U_p - u_{2B}) \left.\right\rbrace \quad \text{PROJECTILE} \qquad (C.3)$$

$$P_{2B} - P_{oB} = \rho_{oB}(U_p - u_o)(u_{2B} - u_o) \qquad (C.4)$$

$$P_{oB} = P_{1A} \approx 0. \qquad (C.5)$$

These are the equations which govern the shocks in the target and projectile immediately after the impact between two different materials. Across the interface, we have the conditions

$$u_{2B} = u_{2A} = u_2 \qquad (C.6)$$

$$P_{2B} = P_{2A} = P_2 . \qquad (C.7)$$

81

PLANE SHOCK AND LATE-STAGE EQUIVALENCE

Combining eqs. (C.2), (C.4), (C.5), (C.6), and (C.7) gives

$$u_2 U_t = \frac{\rho_{OB}}{\rho_{1A}} (u_o - U_P)(u_o - u_2).\qquad(C.8)$$

The shock velocity in the target, U_t, can be related to u_2 by the Hugoniot eq. (18) for the target material. For the projectile, the corresponding Hugoniot must be written in terms of the shock and the particle velocities, relative to the material ahead of the shock, or

$$(u_o - U_P) = b_{1B} + b_{2B}(u_o - u_2) + b_{3B}(u_o - u_2).\,(C.9)$$

With both U_t and U_p expressed in terms of u_2, equation (C.8) may be used to solve for u_2 at a given value of u_o. Once u_2 is known, the characteristics in the P,u-plane are plotted from eq. (15a), with the proper values of A', γ, and P_o.

DISTRIBUTION LIST

Director of Defense Research &
    Engineering (OSD)
Washington 25, D. C.

Commanding Officer
Diamond Fuze Laboratories
Attn: Technical Information Office
        Branch 012
Washington 23, D. C.

Commanding General
Frankford Arsenal
Attn: Library Branch, 0270
        Building 40
Philadelphia 37, Pennsylvania

Commanding Officer
Rock Island Arsenal
Rock Island, Illinois

Commanding Officer
Watervliet Arsenal
Watervliet, New York

Commanding Officer
Watertown Arsenal
Watertown 72, Massachusetts

Commanding Officer
U. S. Army Chemical Warfare
        Laboratories
Edgewood Arsenal, Maryland

Commanding General
Engineer Research & Development
        Laboratories
U. S. Army
Fort Belvoir, Virginia

Commanding General
U. S. Army Signal Engineering
        Laboratories
Fort Monmouth, New Jersey

Professor of Ordnance
U. S. Military Academy
West Point, New York

Chief, Bureau of Naval Weapons
Attn: RIB-33
Department of the Navy
Washington 25, D. C.   (4)

Commander
U. S. Naval Weapons Laboratory
Dahgren, Virginia

Commanding Officer
David W. Taylor Model Basin
Washington 7, D. C.

Commander
U. S. Naval Ordnance Laboratory
White Oak
Silver Spring 19, Maryland   (2)

Commander
U. S. Naval Missile Center
Point Muga, California

Commander
Air Force Cambridge Research
            Laboratories
L. G. Hanscom Field
Bedford, Massachusetts

Commander
Air Force Special Weapons Center
Kirtland Air Force Base, N. Mex.

U. S. Atomic Energy Commission
Los Alamos Scientific Laboratory
P. O. Box 1663
Los Alamos, New Mexico

U. S. Atomic Energy Commission
Attn: Technical Reports Library
Washington 25, D. C.

U. S. Atomic Energy Commission
Lawrence Radiation Laboratory
P. O. Box 808
Livermore, California

Director
Advanced Research Projects Agency
Attn: Mr. James Blower
Washington 25, D. C.   (2)

Director
NASA
Langley Research Center
Langley Field, Virginia

Director
NASA
Lewis Research Center
21000 Brookpark Blvd.
Cleveland 35, Ohio

Commanding Officer
Picatinny Arsenal
Attn: Feltman Research and
       Engineering Laboratories
Dover, New Jersey

Research Analysis Corporation
Attn: Document Control Office
6935 Arlington Road
Bethesda, Maryland
Washington 14, D. C.

Director
U. S. Naval Research Laboratory
Washington 25, D. C.

Commander
Air Proving Ground Center
Eglin Air Force Base, Florida

Commander
Aeronautical Systems Division
Wright-Patterson Air Force Base,
Ohio

Director, Project RAID
Department of the Air Force
1700 Main Street
Santa Monica, California

Director
NASA
Attn: Chief, Division of
       Research Information
1520 H. Street, N. W.
Washington 25, D. C.

U. S. Department of Interior
Bureau of Mines
Attn: Chief, Explosive and
       Physical Sciences Div.
Pittsburgh 13, Pennsylvania

Library of Congress
Technical Information Division
Attn: Bibliography Section
Reference Department
Washington 25, D. C.

Director
Applied Physics Laboratory
The Johns Hopkins University
8821 Georgia Avenue
Silver Spring, Maryland
THRU: Naval Inspector of Ordnance
       Applied Physics Laboratory
       The Johns Hopkins University
       8621 Georgia Avenue
       Silver Spring, Maryland

Firestone Tire and Rubber Compnay
Akron 17, Ohio
Attn: Librarian
       Mr. M. C. Cox
       Defense Research Division

Carnegie Institute of Technology
Department of Physics
Pittsburgh 13, Pennsylvania
Attn: Prof. Emerson M. Pugh
THRU: Commanding Officer
       Philadelphia Procurement
                District
       128 North Broad Street
       Philadelphia 2, Pennsylvania

The General Electric Company
Missiles and Space Vehicles Division
3198 Chestnut Street
Philadelphia 4, Pennsylvania
Attn: Mr. E. Bruce
      Mr. Howard Semon

Chief of Research and Development
Attn: Army Research Office
Department of the Army
Washington 25, D. C.

General Motors Corporation
Defense System Division
Box T
Santa Barbara, California

U. S. Geological Survey
Department of the Interior
4 Homewood Place
Menlo Park, California

Director
NASA
Ames Research Center
Moffet Field, California

Explosives Research Group
University of Utah
Salt Lake City, Utah

Poulter Laboratories
Stanford Research Institute
Menlo Park, California

High Velocity Laboratory
University of Utah
Salt Lake City, Utah

Aeroelastic and Structures
   Research Laboratory
MIT
Cambridge 39, Massachusetts

Division of Engineering
Brown University
Providence, Rhode Island

General Atomics Division
General Dynamic Corporation
Attn: Dr. M. Walsh
San Diego, California

Stevens Institute of Technology
Davidson Laboratory
Castle Point Station
Hoboken, New Jersey

Pratt and Whitney Aircraft
Attn: Mr. Harry Kraus
East Hartford 8, Connecticut

Defense Documentation Center
Attn: TIPCR
Cameron Station
Alexandria, Virginia   (20)

Commanding Officer
Ballistic Research Laboratories
Attn: AMKER-TD
      Dr. Floyd E. Allison
Aberdeen Proving Ground
Maryland   (30)